



RESEARCH ARTICLE

Astrobiological applications of μ -mapping X-ray fluorescence spectrometry

David Frederick Blake¹ , Richard C. Walroth¹, Thomas F. Bristow¹, Philippe Sarrazin², Marc Gailhanou³, Kathleen Thompson⁴, Robert Terrance Downs⁵, Albert Shi-Yuen Yen⁶, Franck Marchis⁴, Samuel Webb⁷, Clement Chalumeau², Vincente Armando Solé⁸ , Philippe Walter⁹, Jianxin Chen¹⁰, Roger Henderson¹¹ and Barbara Lafuente⁴

¹Space Science Division, NASA Ames Research Center, Moffett Field, CA 94035, USA

²eXaminArt, LLC, Mountain View, CA, USA

³CNRS, IM2NP, Aix Marseille Université Institut Universitaire de Technologie de Marseille, Marseille, France

⁴SETI Institute, Mountain View, CA, USA

⁵Department of Geological Sciences, University of Arizona, Tucson, AZ, USA

⁶Jet Propulsion Laboratory, Earth and Space Sciences, NASA-JPL, Pasadena, CA, USA

⁷Stanford Synchrotron Radiation Facility, Stanford University, Stanford, CA, USA

⁸European Synchrotron Radiation Facility, Grenoble, France

⁹Faculty of Science and Engineering, CNRS – Sorbonne Université, Paris, France

¹⁰Baja Technology, LLC, Tucson, AZ, USA

¹¹Radiochemistry, Lawrence Livermore National Laboratory, Livermore, CA, USA

Corresponding author: David Frederick Blake; Email: david.blake@nasa.gov

Received: 11 November 2023; **Accepted:** 17 January 2024

Keywords: elemental imaging, geochemistry, habitability, Mars, X-ray fluorescence spectroscopy

Abstract

In situ elemental imaging of planetary surface regolith at a spatial resolution of 100s to 1000s of microns can provide evidence of the provenance of rocks or sediments and their habitability, and can identify post-depositional diagenetic alteration affecting preservation. We use high-resolution elemental maps and XRF spectra from MapX, a flight prototype *in situ* X-ray imaging instrument, to demonstrate this technology in rock types relevant to astrobiology. Examples are given for various petrologies and depositional/diagenetic environments, including ultramafic/mafic rocks, serpentinites, hydrothermal carbonates, evaporites, stromatolitic cherts and diagenetic concretions.

Contents

Introduction	2
The value of microscale <i>in situ</i> observations of planetary surfaces	2
Micro-mapping X-ray fluorescence spectrometry (μ -mapping XRF)	2
Materials and methods	3
Results	5
Ultramafic xenoliths from Spitsbergen, Norway; analogues of the ALH84001 meteorite	6
Serpentinization of mafic and ultramafic rocks: a source of energy for chemosynthetic ecosystems	6
Carbonates on earth and Mars	9
Ancient cherts: fine-scale early preservation of evidence of life and habitability	12

Evaporites	14
Hematite/goethite diagenetic crystallization	14
Discussion	15
Conclusions	17

Introduction

The value of microscale in situ observations of planetary surfaces

Many low-temperature planetary surface processes leave traces of their actions as features in the size range from 0.01 mm to several mm. Syn-sedimentary, authigenic and diagenetic features at the higher end of this size range include varves, vesicles, precipitates and concretions that can be used to decipher depositional and diagenetic processes. On the Earth, microbial life is known to exploit microscale disequilibria at boundaries where valence, chemical potential, pH, Eh, etc., vary on a length scale commensurate with the organisms themselves – tens to thousands of micrometres. These disequilibria can exist within cracks or veins in rocks and ice, at inter- or intra-crystalline boundaries, at sediment/water or sediment/atmosphere interfaces, or within fluid inclusions trapped inside minerals. Larger organized sedimentary structures such as stromatolites can provide macroscale evidence of biogenic influence, but abiotic examples are known as well and detailed study at the microscale is required for confirmation of biogenicity. Detection of accumulations of the biogenic elements C, N, O, P and S at appropriate concentrations on or in a mineral substrate could constitute permissive evidence of life, but context is also necessary. Does or did the putative biosignature exist in a habitable environment? Under what conditions of P, T and chemical potential was the host mineralogy formed? Most importantly, post-emplacement alteration (taphonomy) resulting from variations in temperature, pressure or fluid chemistry after deposition has the capacity to preserve evidence of biogenicity or its processes, or to erase such evidence completely.

In the characterization of solids (rocks, soil or planetary regolith), three fundamental properties can be used to elucidate conditions of formation and post-formational processing history: *crystal structure*, *elemental composition* and *morphology*. Based on these measurable properties, it is possible to determine provenance (useful in evaluating habitability or biogenicity) and taphonomy (useful in evaluating preservation potential).

Micro-mapping X-ray fluorescence spectroscopy (μ -mapping XRF)

The Mars Exploration Rovers *Spirit* and *Opportunity* each had instruments capable of elemental analysis (Alpha Particle X-ray Spectrometer (APXS); Rieder *et al.*, 2003; Gellert *et al.*, 2006), iron mineralogy (Mössbauer Spectrometer; Morris *et al.*, 2006), IR imagery (Miniature Thermal Emission Spectrometer (Mini-TES); Christensen *et al.*, 2003; Ruff *et al.*, 2006) and contextual hand-lens imagery (Athena Microscopic Imager (MI); Herkenhoff *et al.*, 2003; Herkenhoff *et al.*, 2008). The spatial resolution of all but the microscopic imager is on the order of centimetres, with the result that imaged features can rarely be related to elemental chemistry or mineralogy. The Mars Science Laboratory rover *Curiosity* (Grotzinger *et al.*, 2012) is capable of landed optical imagery of rocks or soil with an ultimate spatial resolution of tens of microns (Mars Hand Lens Imager (MAHLI); Edgett *et al.*, 2012), and quantitative compositional data can be obtained from quite larger surface areas of 2–3 cm diameter using APXS (Campbell *et al.*, 2012). Occasionally, smaller features of a few mm have been characterized by comparing data from areas of regolith on and off a feature of interest (VanBommel *et al.*, 2016). The Laser-Induced Breakdown Spectrometry (LIBS) instrument on *Curiosity* (Maurice *et al.*, 2012) is capable of acquiring sub-mm qualitative to semi-quantitative elemental information, but these data are limited to individual spots and 1D or 2D arrays of analyses that are rudimentary at best when compared to companion optical information. Mineralogical data from the Chemistry and Mineralogy (CheMin) instrument (Blake *et al.*, 2012) and the Surface Analysis at Mars (SAM) instrument (Mahaffy *et al.*, 2012) represent a homogenized volume of soil collected by a

scoop, or a powdered drill core 1 cm in diameter and 3–6 cm deep (Sample Acquisition, Sample Processing and Handling (SA/SPaH) instrument; Anderson *et al.*, 2012).

The PIXL instrument on the Mars 2020 rover *Perseverance* (Allwood *et al.*, 2020) for the first time provided a capability to X-ray map and quantitatively analyse a small portion of Mars regolith with 125 μm lateral spatial resolution (see e.g. Liu *et al.*, 2022; Tice *et al.*, 2022; Scheller *et al.*, 2023). PIXL is a scanning instrument in which a focused 125 μm diameter X-ray beam is moved in X and Y across a regolith surface. Two silicon drift detectors (SDD) collect the fluoresced X-rays as the beam is moved, to produce point analyses, transects or X , Y elemental maps. The ultimate resolution of the analysis is defined by the distance between the X , Y positions.

A second method of X-ray mapping utilizes a flood of X-rays/ γ -rays/ α -particles to irradiate the entire sample at once, and an X-ray lens to focus the fluoresced photons from the sample onto a charge coupled device (CCD) detector. This method is called full-frame X-ray fluorescence imaging (FF-XRF). FF-XRF instruments have been demonstrated in space (Mercury Imaging X-ray Spectrometer (MIXS); Fraser *et al.*, 2010) in the laboratory (Price *et al.*, 2004), as planetary instrument prototypes (Mapping X-ray Spectrometer (MapX); Blake *et al.*, 2015; Sarrazin *et al.*, 2016, 2018; Thompson *et al.*, 2017; Walroth *et al.*, 2019) and as portable field instruments (MapX-II (Cartix); Walter *et al.*, 2018; Sepúlveda *et al.*, 2020).

Irrespective of how X-rays are detected and imaged, with a full characterization of the excitation source and source–sample–detector geometry, it is possible to calculate spatially resolved quantitative compositional information using the fundamental parameters method (Solé *et al.*, 2007; Pia *et al.*, 2009; Schoonjans *et al.*, 2012).

Here we present elemental imaging results from a variety of sample types relevant to astrobiology, collected at $\sim 125 \mu\text{m}$ lateral resolution in MapX-III, a FF/XRF planetary instrument prototype. These data are compared with imaging results collected at 50 μm lateral spatial resolution in a commercial scanned beam X-ray imaging instrument (EDAX Orbis).

Materials and methods

Hand samples, thin sections and thin section stubs were selected that represent a range of habitable environments, diagenetic fabrics and biologically mediated structures. Bulk samples were trimmed to petrologic thin-section size ($19 \times 26 \text{ mm}$) and thin sections were prepared. The prepared slides are intended to represent the smooth and dust-free abrasion targets typically studied by the Mars 2020 *Perseverance* rover's X-ray fluorescence (PIXL) and Raman (SHERLOC) microscale mapping instruments (Hickman-Lewis *et al.*, 2022; Razzell *et al.*, 2022). In addition, thin sections allow for a petrographic characterization of the samples, useful for relating underlying microstructures with X-ray fluorescence maps. Representative portions of each sample were powdered and analysed by X-ray diffraction to determine the quantitative mineralogy of the samples.

Samples were first imaged and analysed in a commercial EDAX Orbis X-ray spectrometer in vacuum under a standard set of conditions: accelerating voltage 30 keV, beam current 350 μA (10.5 W), rhodium anode, 30 μm spot size polycapillary optic, 80 mm^2 SDD detector. Samples were scanned with a step size of 50 μm , and a dwell time of 0.2 s. In a typical analysis of a $19 \times 26 \text{ mm}$ thin section, a matrix of 380×520 spots is collected, requiring $\sim 11 \text{ h}$ and 115 Watt hours (Wh) total beam energy.

The geometry of the MapX instrument used in this work is illustrated in Fig. 1. Sources bombard the sample with X-rays or α -particles/ γ -rays, resulting in sample X-ray fluorescence (data for all figures in this paper were collected in MapX-III, a prototype having X-ray tube sources). X-ray photons emitted in the direction of an X-ray sensitive CCD imager pass through a 1:1 lens (X-ray Micro-Pore Optic (MPO)) that focuses a spatially resolved image of the X-rays onto the CCD. The CCD is operated in single photon counting mode (meaning that the imager is read often enough so that in the vast majority of cases, each pixel in the array contains either the charge generated by a single photon, or background). Under these conditions, both the energies and X , Y positions of individual X-ray photons are recorded. In a single analysis, several thousand frames are collected and processed in real time.

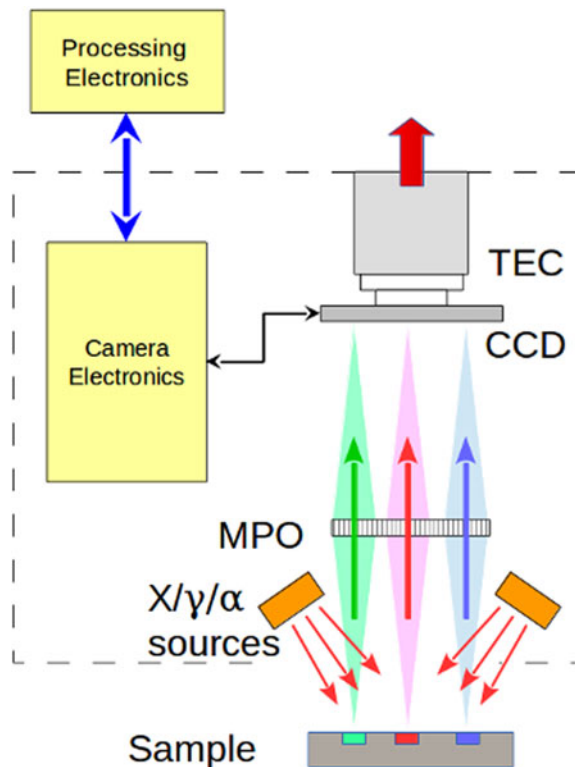


Figure 1. Schematic diagram of the MapX instrument. X-ray or radioisotope sources fluoresce the sample. Fluoresced X-ray photons characteristic of elements present in the sample are emitted over 2π steradians from their point of origin on the surface. Photons that enter the MPO within its acceptance angle are focused onto an energy-discriminating X-ray sensitive CCD in a 1:1 configuration with the sample. Hundreds to thousands of short exposures, each one a complete 2D X-ray image of the sample, are summed to produce an hdf5 data file.

MapX-III (Fig. 2) is comprised of custom flight-qualifiable camera electronics that drive a flight-qualified e2v frame-transfer front illuminated CCD-224. The camera is interfaced to a high vacuum enclosure that contains the CCD-224 imager, a Photonis MPO lens and sample stage. Two Newton Scientific Au target transmission window X-ray tubes, operated at 15 keV and 25 μ A (0.750 W total) illuminate the sample through ports in the chamber.

The overall geometry of the instrument (distances between sample, MPO and CCD, and the characteristics of the MPO) was optimized through the testing of MPO lenses at Stanford Synchrotron Radiation Light Source Beam Line 2-3 (Sarrazin *et al.*, 2018) and by ray-tracing simulations (Gailhanou *et al.*, 2018). The measured lateral spatial resolution of the instrument is 100 μ m with a depth of field of ± 5 mm with minimal loss of resolution.

Samples were imaged and analysed in MapX-III under the conditions noted in the text for each analysis. The equivalent of ≤ 3 h of analysis time is considered as a nominal baseline for a deployed planetary instrument. MapX can be equipped with either an X-ray tube source or a radioisotope source to fluoresce the sample. For an X-ray tube sourced instrument, we modelled 25 KeV accelerating voltage and 200 μ A beam current (5 W total power in the beam, 15 Wh total energy per analysis). For a radioisotope sourced instrument, we modelled 30 mCi of ^{244}Cm , equivalent to that used in the APXS instruments (Rieder *et al.*, 2003; Gellert *et al.*, 2006; Economou, 2011). The radioisotope ^{244}Cm produces 14 and 18 KeV γ -rays (suitable for fluorescing $K\alpha$ lines from calcium through zirconium) and 5.8 MeV α -particles (suitable for fluorescing $K\alpha$ lines from oxygen through potassium).

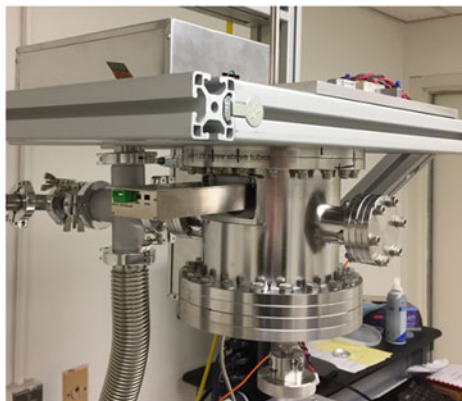
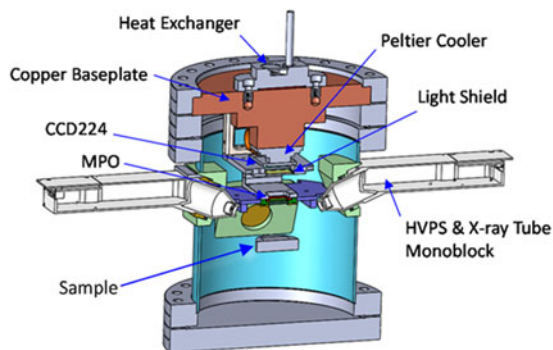


Figure 2. (a). Cross-section of MapX-III prototype, showing sample position, X-ray tubes, MPO and CCD224 imager in an evacuated chamber. (b). MapX-III prototype. With the exception of the X-ray tubes, MapX-III is assembled from flight qualified or qualifiable components: two Newton Scientific M54 Au target transmission X-ray tubes; an e2v front illuminated, deep depleted frame transfer CCD-224 (legacy from CheMin, 600×600 $40 \mu\text{m}$ pixels); and an Ir coated 1.5 mm thick MPO with $20 \mu\text{m}$ square channels and $6 \mu\text{m}$ thick walls. Samples in MapX-III are held in the same vacuum as the CCD, eliminating the need for a Be window and allowing for element detection down to $Z = 11$ (Na). MapX-III has a lateral spatial resolution of $\sim 125 \mu\text{m}$ and an energy resolution of $\sim 200 \text{ eV}$.

Whether from the EDAX instrument or MapX-III, once data are collected, they are processed identically. In MapX-III, the individual images (frames) collected by the CCD are binned by energy and combined into an $X \times Y \times \text{photon energy}$ hdf5 data cube (see Supplementary Information and Fig. S1). The data cube is commonly hundreds of megabytes in size, too large for routine downlink from a spacecraft. Software was developed to generate reduced data records more suitable for downlink. Single-element maps, Mg–Ni are computed from the hdf5 file using custom python code. These maps are qualitative only in that fluorescence efficiency, absorption effects, detector efficiency, etc., are not accounted for. In a 3 h nominal analysis, single-pixel spectra lack sufficient counting statistics to be quantified. However, qualitative single-element maps are the highest resolution and highest sensitivity data products produced by the instrument.

We use an unsupervised machine learning program to identify regions of similar composition (regions of interest or ‘ROI’) in the hdf5 data cube. ROI are identified by finding element–element correlation clusters in $N \times N$ dimensional space where N is the number of relevant elements (see Supplementary Information and Fig. S2). These clusters are then applied to the 2D image to generate a map of ROI. The XRF spectra from the individual pixels contained in each ROI are summed to generate high signal-to-noise quantifiable XRF spectra for ground processing. The hdf5 data cube is reduced to a set of single-element maps, a set of ROI (composition maps) having unique element compositions and XRF spectra from each ROI. If necessary, the hdf5 data cube can be reprocessed to generate additional data products on the basis of the initial quick-look elemental images and ROI.

Results

Examples are organized by rock type and depositional/diagenetic environment (ultramafic/mafic rocks, serpentinites, hydrothermal carbonates, evaporites, stromatolitic cherts and diagenetic concretions). All raw hdf5 files, element maps, ROI, ROI spectra, etc., for the samples shown here and many others are archived in and downloadable from the Planetary X-ray Fluorescence Petrography database: <https://doi.org/10.48484/R7WV-3T89>.

Ultramafic xenoliths from Spitsbergen, Norway; analogues of the ALH84001 meteorite

Xenoliths of mantle material comprise as much as 20% by volume of several quaternary volcanic centres in Spitsbergen, Norway. The xenoliths include spinel lherzolites and pyroxenites having mineralogies broadly similar to that of the Mars meteorite ALH84001, purported to show evidence of microbial life on ancient Mars (McKay *et al.*, 1996).

While the preponderance of available evidence now supports an abiotic origin for the carbonate globules in ALH84001 (e.g. see Treiman *et al.*, 2002), this meteorite nevertheless represents an important rock type for Mars. The mineralogy/petrology of ALH84001 demonstrates that deep-seated volcanism occurred ~4.1 Gy before the present, influenced by a low-temperature near-surface or surface hydrothermal event predating a shock that caused the ejection of ALH84001 from the planet's surface. The hydrothermal event was brief enough, or at low enough temperature (<<200°C) that the ultramafic minerals, unstable in the presence of water, were not altered to serpentine.

Figure 3 illustrates a partial EDAX and MapX-III dataset from AMASE08 UI-3, one of several ultramafic xenoliths from Spitsbergen, Norway that were analysed by X-ray diffraction, electron microprobe and optical point counting (Treiman *et al.*, 2010). The highest resolution data returned by the instrument are the individual elemental images. ROI representing regions of the sample having common compositions were calculated from the hdf5 data cube using an unsupervised machine learning algorithm (see Supplementary Information and Figs S1 and S2). In this example, ROI are seen to represent three minerals plus basalt: clinopyroxene (cpx, ROI 1), orthopyroxene (opx, ROI 3), chrome spinel (csp, ROI 4) and host basalt (bas, ROI 2). Mineral identifications were made separately on UI-3 thin sections and powder separates using optical point counting, electron microprobe and X-ray diffraction data (enstatite 26.09 wt.%, forsterite 7.79 wt.%, augite 59.22 wt.%, albite 4.05 wt.%, spinel 2.85 wt.%) (Treiman *et al.*, 2010). XRF spectra returned for each ROI can be quantified using fundamental parameters methods, and in favourable cases, it is possible to relate the compositions of ROI to specific minerals using the RRUFF database (Lafuente *et al.*, 2015). Total beam power: 9 Wh, equivalent to 120 min of analysis with a nominal X-ray tube or ²⁴⁴Cm radioisotope-based spacecraft instrument.

It is interesting to note that one of the first rock types imaged in Jezero crater by the PIXL instrument (Farley *et al.*, 2022; Liu *et al.*, 2022) has a similar fabric and mineralogy to the ultramafic xenoliths analysed from Spitzbergen (Treiman *et al.*, 2002, 2010) and illustrated in Fig. 3.

Serpentinization of mafic and ultramafic rocks: a source of energy for chemosynthetic ecosystems

Serpentinization is the process by which ultramafic rocks containing olivine and pyroxene react with water to form magnetite, serpentine and hydroxide minerals. As a consequence of this reaction, molecular hydrogen is released, a potential source of chemical energy for life (McCollom and Shock, 1997; Sleep *et al.*, 2004). Serpentinizing systems are regarded as important analogues for potential early ecosystems on Earth and Mars, where highly reducing mineralogy was likely widespread in an undifferentiated crust (Kelley *et al.*, 2005; Schulte *et al.*, 2006).

The second and third samples collected and analysed by the MSL *Curiosity* rover during its investigation of Gale crater on Mars were of a ~3.7 G-year-old mudstone interpreted to be a lithified sediment deposited in a lacustrine environment (Grotzinger *et al.*, 2013; Vaniman *et al.*, 2013; Bristow *et al.*, 2015). When compared to the elemental composition of global soil (used as a proxy for average Martian basalt) collected during *Curiosity*'s first analysis on Mars (Bish *et al.*, 2013; Blake *et al.*, 2013), the elemental composition of the mudstone (now principally comprised of secondary minerals) is a close match, suggesting that the mudstone was similar in its initial mineralogy and experienced a closed-system diagenetic event. On the basis of mass-balance calculations, Bristow *et al.* (2015) propose a mechanism akin to serpentinization in which original mafic minerals (e.g. olivine), unstable in the presence of water, transformed into a stable assemblage including clay minerals (ferrian saponite; Treiman *et al.*, 2014) and magnetite. Hydrogen would have been released in such a reaction, and on the

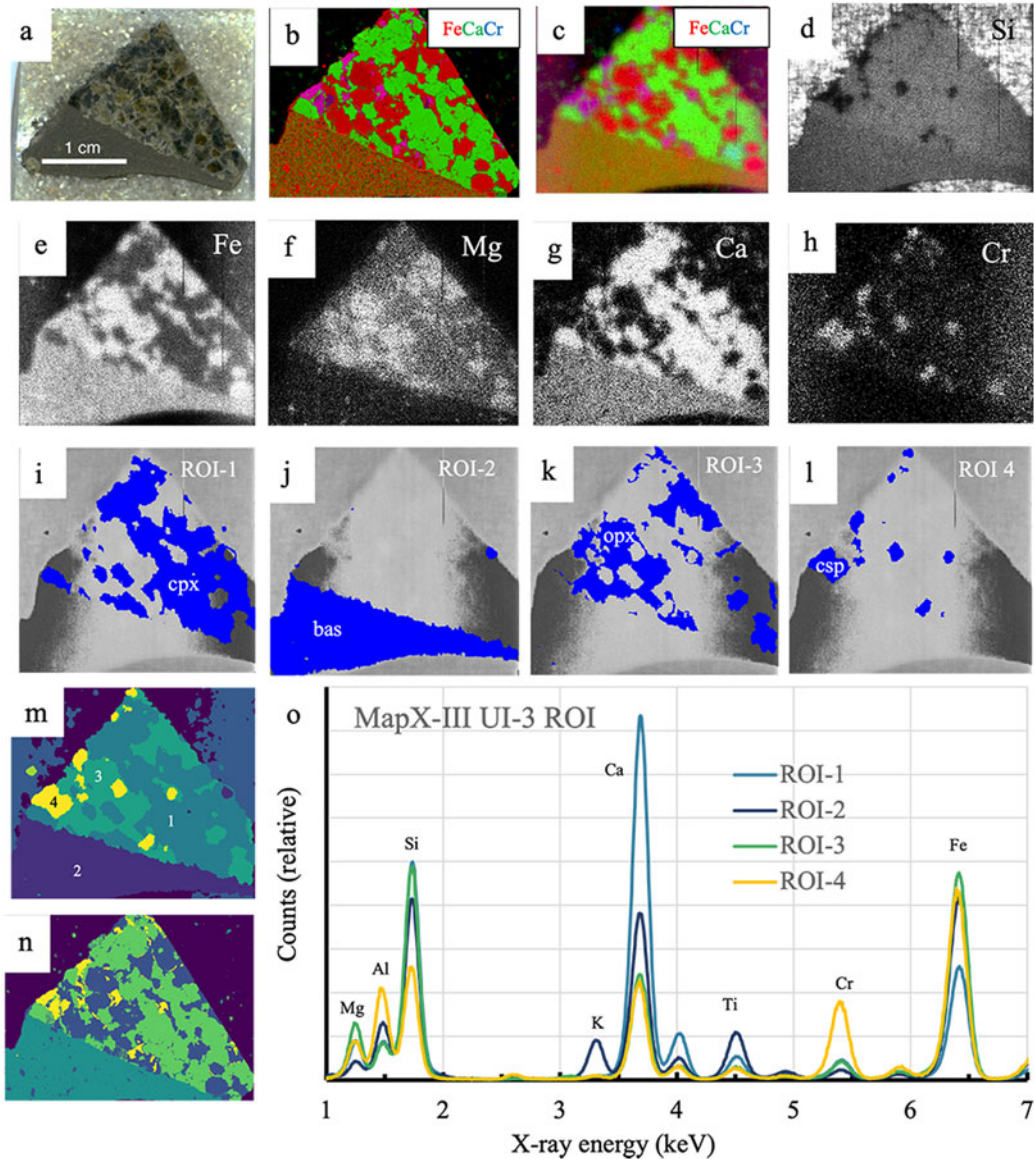


Figure 3. Ultramafic xenolith from Spitsbergen, Norway. (a) Optical image of a thin section stub of ultramafic xenolith AMASE08 UI-3; (b) RGB element map from commercial EDAX-Orbis instrument (50 μm resolution), Red = Fe, Green = Ca, Blue = Cr; (c) RGB element map from MapX-III (~125 μm resolution), same colour scheme as in (b); (d–h) MapX-III elemental maps; (i–l) ROI selected by element correlation cluster analysis from MapX-III hdf5 data cube; (m) ROI map from MapX-III (numbers refer to labelled ROI spectra shown in (o)); (n) ROI map from EDAX (note: colours for ROI-2 and ROI-3 are reversed); (o) summed XRF spectra from individual ROI; ROI 1 = clinopyroxene, ROI 2 = basalt matrix, ROI 3 = orthopyroxene, ROI 4 = chrome spinel (total MapX-III beam power = 9 Wh (120 min analysis)).

basis of the mineral assemblage and its sedimentological context, this ancient lakebed was identified as a habitable environment for chemosynthetic organisms (Grotzinger *et al.*, 2013).

Orbital spectral observations made by the CRISM instrument on Mars Reconnaissance Orbiter have identified serpentine and serpentine-like minerals in many locations on Mars, suggesting the presence

of widespread and deep-seated serpentinization reactions in the crust of Mars, creating potential habitable environments early in Mars history (Ehlmann and Edwards, 2014 and references therein).

The most widespread serpentinizing environment on the Earth is the seafloor, where mafic and ultramafic oceanic crust interacts with seawater (Deming and Baross, 1993; McCollom and Shock, 1997; Kelley *et al.*, 2001a, 2001b). ‘Ophiolite sequences’, slivers of oceanic crust thrust upward into the shallow continental crust as a result of plate tectonics, are found in northern California and southern Oregon (Coleman, 2000). These rocks, in contact with connate fluids at moderate to low temperatures ($\sim 200^{\circ}\text{C}$), are presently undergoing serpentinization (Barnes *et al.*, 1967; Barnes and O’Neil, 1969; Blake and Peacor, 1985).

Schulte *et al.* (2006) analysed hand samples of olivine-rich rocks from actively dewatering outcrops in the Coast Range Ophiolite in N. California. Figure 4 illustrates a partial dataset from a thin section

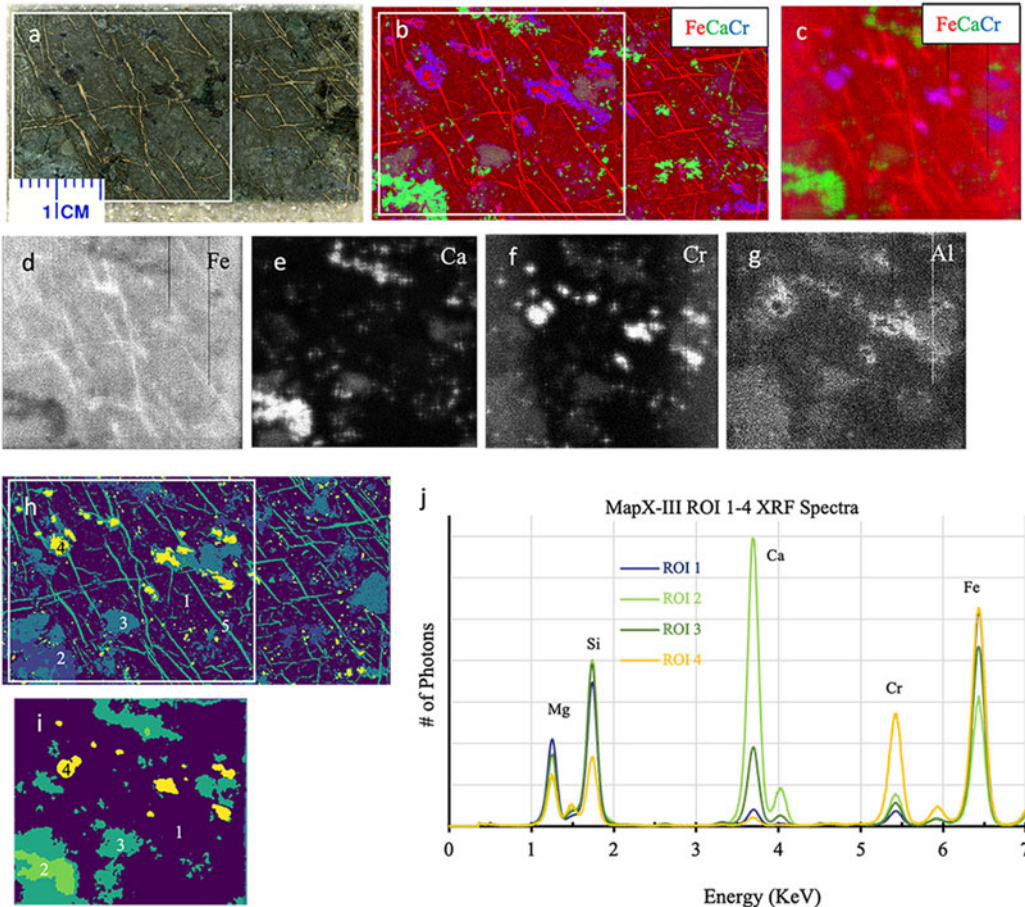


Figure 4. Thin section stub of a partially serpentinized cobble from Complexion Springs, California. (a) Optical image, white rectangle shows area imaged in MapX-III; (b) RGB element map from EDAX-Orbis instrument ($50\ \mu\text{m}$ resolution), Red = Fe, Green = Ca, Blue = Cr; white rectangle shows area imaged in MapX-III; (c) RGB element map from MapX-III ($\sim 125\ \mu\text{m}$ resolution), same colour scheme as in b; (d–g) element images from MapX-III; (h) ROI selected by elemental correlation cluster analysis from EDAX hdf5 data cube (numbers refer to individual ROI also shown in (i) from the MapX-III instrument; (i) ROI selected by elemental correlation cluster analysis from MapX-III hdf5 data cube; (j) MapX-III XRF spectra from individual ROI, numbers refer to ROI labelled in (i) (total MapX-III beam power = 2.25 Wh (30 min analysis)).

stub of one such sample described in Schulte *et al.* (2006). The modal proportions of minerals in the original rock prior to serpentinization were estimated to be 70% olivine, 20% orthopyroxene, 7% clinopyroxene and 3% other minerals. Primary olivine and pyroxene account for about half of the present mineralogy, with a fine-grained groundmass representing the remaining bulk (and comprised of serpentine minerals, fine-grained magnetite and Fe-rich brucite). Despite the fact that most mineral phases are below the resolution of both the EDAX and MapX-III, the mafic-ultramafic elemental composition of ROI and the rock fabric displayed in element images (secondary veining and the absence of large crystals) strongly suggest that this rock is a serpentinite, and represents a potentially habitable environment.

Carbonates on earth and Mars

Carbonates are important rock-forming minerals on early Earth and should have been on early Mars as well. On early Mars, a dense, CO₂-rich atmosphere in the presence of surface and near-surface water would promote the dissolution of mafic minerals by carbonic acid and the precipitation of Ca-Fe-Mg carbonates at near-normal pH.

Meteoritic carbonates

Carbonates were described in the Martian meteorites Nakhla (Bridges and Grady, 2000; Bridges and Schwenzer, 2012) and in ALH84001 (McKay *et al.*, 1996). While these carbonates comprise a volumetrically small fraction of the overall mineralogy in these meteorites, they are nevertheless important because detailed information about their paragenesis has been obtained with laboratory-based instrumentation. In all cases, carbonate formation can best be explained by surface or near-surface hydrothermal activity in mafic or ultramafic rocks (Bridges *et al.*, 2018 and references therein). Treiman *et al.* (2002) describe carbonate globules contained within ultramafic xenoliths from the Sverrefjell volcano (Spitsbergen, Norway) that are nearly identical to those found in the ALH84001 meteorite and present evidence that the globules are hydrothermal precipitates formed within a shallow sub-surface volcanic complex. Figure 5 shows data from ultramafic xenolith AMASE08 UI-6. X-ray diffraction analysis shows it to be comprised of 15.7% enstatite, 81.1% olivine, 1.9% augite and 1.2% albite. In this case (unlike AMASE08 UI-3 shown in Fig. 3), only a small amount of Ca-containing clinopyroxene is present, so that carbonate globules are identifiable based on Ca element images. Treiman *et al.* (2010) describe the secondary mineralization shown in (Fig. 5(f)) as partial melts and products of aqueous alteration near and around spinels, the alteration products including zoned spherules of (CaMg,Fe)CO₃.

Martian carbonates

Orbital observations of Mars with the Compact Reconnaissance Imaging Spectrometer for Mars (CRISM) instrument have identified volumetrically significant deposits of carbonate in Nili Fossae (Ehlmann *et al.*, 2008) and elsewhere. Morris *et al.* (2010) report the discovery of carbonate-rich basaltic outcrops in Gusev crater, Mars using instruments aboard the Mars Exploration Rover *Spirit*. Comanche Spur is an apparent volcanoclastic deposit with a fracture filling comprised of Mg-Fe-Ca carbonate. The composition of the carbonate is reported to be Mg_{0.62}Fe_{0.25}Mn_{0.02}Ca_{0.11}CO₃ based on Mossbauer, APXS and Mini-TES instrumental data. The closest terrestrial analogue to the Comanche carbonate is from Spitsbergen, Norway in carbonate-cemented, breccia-filled volcanic pipes associated with late-stage hydrothermal activity. Morris *et al.* (2011) describe this occurrence (see also Treiman *et al.*, 2010; Blake *et al.*, 2011). The Sverrefjell volcanic province is quaternary in age and manifests itself as volcanic cinder cones which on the basis of pillow basalts exposed on their flanks, must have erupted under water (Treiman *et al.*, 2002). Laboratory and field evidence

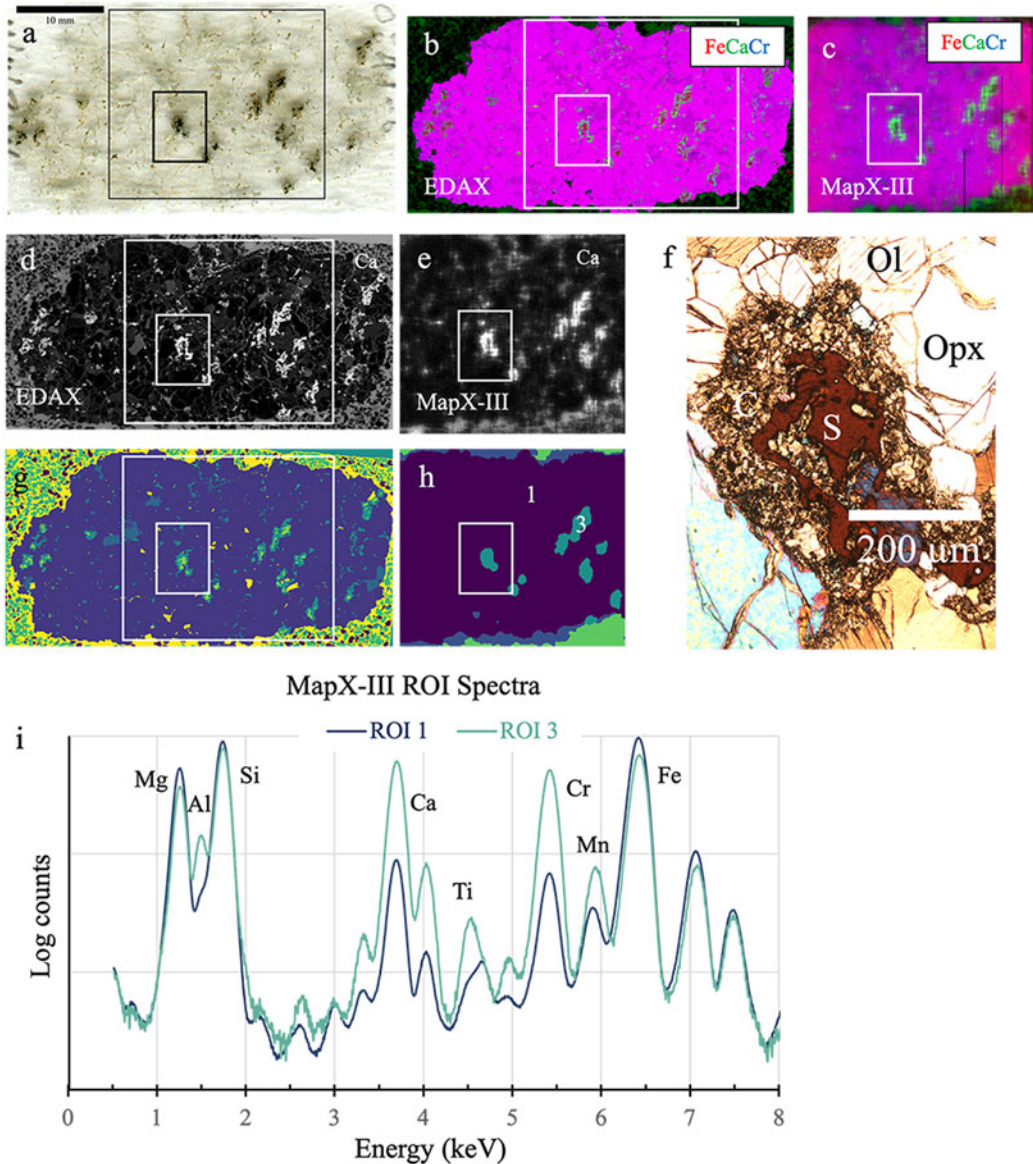


Figure 5. Ultramafic xenolith AMASE UI-6, an orthopyroxenite comprised principally of orthopyroxene and olivine with minor chrome spinel and carbonate. (a) Petrographic thin section, small black rectangle shows area of thin section magnified in (f); (b) RGB element map from EDAX-Orbis instrument, Red = Fe, Green = Ca, Blue = Cr, large white rectangle shows area imaged in MapX-III; (c) RGB element map from MapX-III, colour scheme same as in (b); (d) Ca element image from EDAX instrument; (e) Ca element image from MapX-III instrument; (f) optical micrograph of portion of thin section outlined in figures a–e, g, h, showing carbonates (C) and other secondary mineralization surrounding chrome spinel (S), Opx – orthopyroxene, Ol = olivine; (g) ROI map from EDAX instrument; (h) ROI map from MapX-III instrument; (i) XRF spectra from MapX-III ROI labelled 1 and 3 in (h) (total beam power = 9 Wh (120 min analysis)).

suggest that the carbonates were deposited by hydrothermal fluids, likely heated by the volcanic rock itself, flowing through pre-existing volcanic pipes in a hydrothermal cell. Figure 6 shows EDAX and MapX results from a thin section of a carbonate-cemented basalt breccia from this locality. At the 50 μm spatial resolution of the EDAX instrument, the prismatic texture of the cement is evident, as are void spaces, demonstrating rapid crystal growth in a surface or shallow sub-surface aqueous environment. At the 125 μm resolution of MapX-III, void spaces are evident, but not the prismatic texture. Elemental maps document changes in carbonate chemistry during cement deposition, and the predominance of the divalent cations Ca-Mg-Mn suggest that the carbonate is rhombohedral. In fact, XRD analyses of these cements (Blake *et al.*, 2011) reveal a wide variety of rhombohedral carbonates, including Mg-calcite ($\text{Mg}_x\text{Ca}_{1-x}\text{CO}_3$), huntite ($\text{Mg}_3\text{Ca}(\text{CO}_3)_4$), magnesite (MgCO_3), dolomite/ankerite ($\text{Ca}(\text{Mg},\text{Fe})(\text{CO}_3)_2$), siderite (FeCO_3) and in some cases late-stage aragonite (orthorhombic CaCO_3). From these data, it appears that specific carbonate mineral chemistries (e.g. thin rind of Mn, calcium core, magnesium rim in the cement) are reflective of changing hydrothermal conditions and what divalent cations are present in the solution.

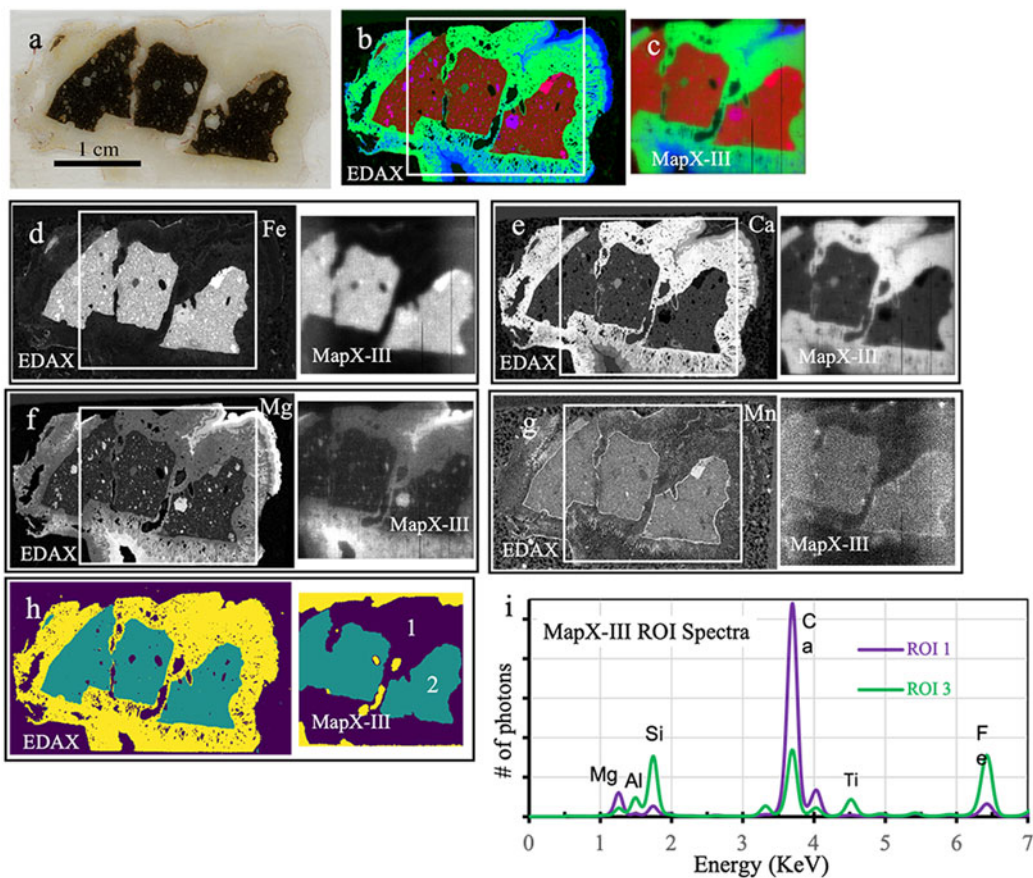


Figure 6. Carbonate-cemented basalt breccia from Spitsbergen, Norway. (a) Petrologic thin section; (b) RGB element map from EDAX-Orbis instrument (50 μm resolution), Red = Fe, Green = Ca, Blue = Mg, white rectangle shows area imaged in MapX-III; (c) RGB element map from MapX-III, same colour scheme as b; (d–g) Element images from EDAX (l) and MapX-III (r); (h) ROI map from EDAX (l) and MapX-III (r) note that ROI 1 from MapX is blue while the same ROI in EDAX is yellow; (i) ROI XRF spectra for MapX-III, ROI labelled in (h) (total beam power = 9 Wh (120 min analysis)).

Ancient cherts: fine-scale early preservation of evidence of life and habitability

On the early Earth, Proterozoic silica deposition (abiotic silica precipitation as either a primary chemical sediment or as an early diagenetic cement in the marine environment) is a predominant mechanism for fine-scale preservation of primary depositional fabrics, early diagenetic features and remnants of the earliest microbial life (cellular processes and organic biosignatures). Original silica was emplaced as amorphous and/or sparingly crystalline opal-A and opal-CT from a silica-saturated ocean (or from silica-rich ground water). These original components have been recrystallized into microcrystalline quartz (i.e. chert) in the rock record. Knoll (1985) suggests that well-preserved stromatolytic occurrences such as the Gunflint Chert (Tyler and Barghoorn, 1954; Barghoorn and Tyler, 1965; Awramik, 1976) were formed in peritidal environments in which evaporation and heightened salinity played a role in silica deposition. It appears that the presence of organic material is a common feature in early silicification, and petrographic observations of cement fabric suggest that initial opal-A or opal-CT nucleation occurs on individual microbial sheaths and processes. A second type of early silica deposition with fine-scale preservation involves the replacement of pre-existing carbonate completely or partially by silica.

Silica deposition as a chemical sediment or an early diagenetic replacement cement should have been common on early Mars, where water interacted with mafic rocks, dissolving olivine, pyroxene and other minerals with the liberation of aqueous silica (McLennan, 2003). Tosca and Knoll (2009) and references therein document numerous detections of hydrated silica on the surface of Mars from both *in situ* and remote observations. For example, evaporative sedimentary rocks at Meridiani Planum contain as much as 20 wt.% hydrated silica (McLennan *et al.*, 2005), and opaline silica was identified in the Columbia Hills of Gusev Crater, interpreted as the product of aqueous activity, possibly related to hydrothermal processes (Squyres *et al.*, 2008). Remote observations from MRO/CRISM have identified opaline silica (Milliken *et al.*, 2008) as well.

The discovery of amorphous and crystalline silica in ~3.5 Ga Murray formation lacustrine mudstone sequences in Gale crater on Mars (Morris *et al.*, 2016; Rampe *et al.*, 2017) raises the possibility that retention of depositional/early diagenetic features in silica (including preservation of organic biosignatures, if present) is possible and even likely on Mars. Silica-rich sequences of the Murray formation (and of other similar sedimentary deposits found elsewhere on Mars) may have the highest probability of retention of evidence of biogenicity (or of abiotically produced endogenous/exogenous carbon) and may offer a taphonomically favourable window into the biologic potential of early Mars.

Figure 7 shows a thin section stub of finely preserved stromatolitic material from the 2.1 Ga Gunflint Chert, Schrieber Beach locality. The chert preserves carbonate features that were likely the original material of the stromatolitic structures. However, abiotically precipitated silica is ubiquitous in the Precambrian, and locations such as Schrieber Beach were only found through extensive fieldwork by paleontologists (and indeed, much of the Gunflint formation was subject to extremes of diagenesis that would have overprinted the features preserved in the Schrieber Beach locality). As shown in the figure, spatially resolved element images can be highly useful in identifying the small fraction of chert samples that may contain evidence of early preservation and of potential biogenicity. It is interesting to note that there are no mineral phases in this sample that are large enough to be resolved by the 125 μm spatial resolution of MapX-III or even the 50 μm spatial resolution of the EDAX instrument (e.g. the Ca-Fe-Mn rich regions in this sample were found by optical microscopy to be comprised of clusters of ~10 μm carbonate rhombs, and the fabric of the microcrystalline chert is only resolvable in a petrographic microscope). The key feature of this sample that would separate it from others is the apparent chemical disequilibrium and heterogeneous distribution of elements in the images and the composition of the ROI at mm- and larger scales.

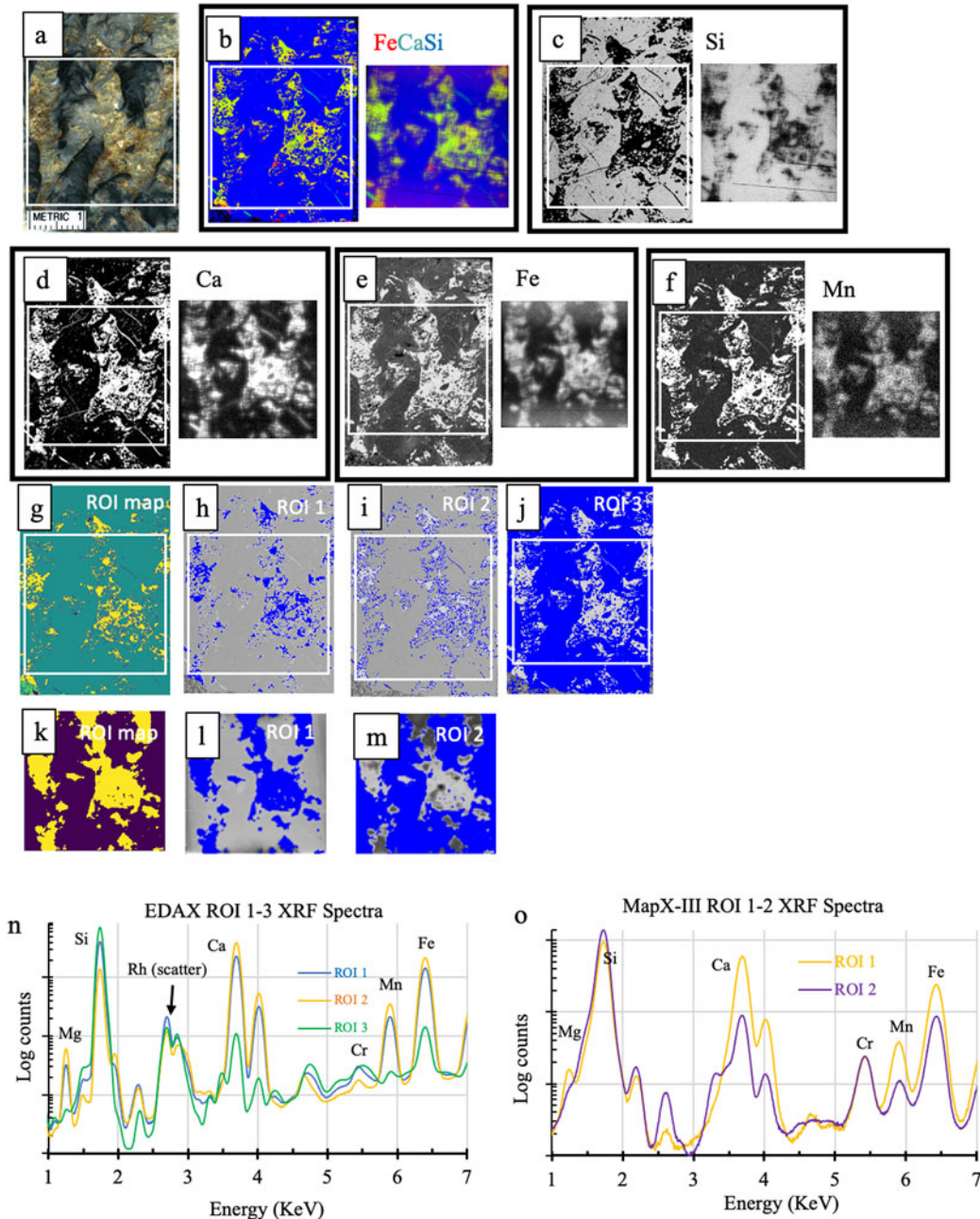


Figure 7. Gunflint Chert, Schrieber Beach locality stromatolite. (a) Polished thin section stub; (b) RGB element maps from EDAX-Orbis and MapX-III instruments, Red = Fe, Green = Ca, Blue = Mg; (c–f) comparison element images from EDAX (l) and MapX-III (r) for Si, Ca, Fe and Mn; (g–j) ROI maps from EDAX instrument; (k–m) ROI maps from MapX-III; (n) XRF spectra for EDAX ROI; (o) XRF spectra for MapX-III ROI (total beam power = 9 Wh (120 min analysis)).

Evaporites

On early Mars, volcanic sulphur emanations combined with the presence of surface water suggest that sulphates of all kinds should be present on the surface. Indeed, on the basis of extensive observations of sulphates from orbit by the OMEGA instrument (Bibring *et al.*, 2006), sulphate deposits are known in the Vallis Marineris (Juventae Chasma), Terra Meridiani (Squyres *et al.*, 2006) and many other places on the Mars surface. In Juventae Chasma, these deposits are over 2 km thick and have an unknown origin (Bishop *et al.*, 2009). MSL's landing site in Gale crater was chosen in part because the central mound of the crater (Mt. Sharp) is comprised of flat-lying phyllosilicate-rich sediments overlain by a sulphate layer (Milliken *et al.*, 2010). During MSL's traverse, gypsum, bassanite and anhydrite have been detected in secondary diagenetic veins and fillings during its entire traverse of the crater. Most recently, the mineral Starkeyite ($\text{MgSO}_4 \cdot 4\text{H}_2\text{O}$) and an amorphous Mg-sulphate were identified by the CheMin XRD instrument on the *Curiosity* rover (Chipera *et al.*, 2023). Starkeyite was seen to dehydrate to amorphous Mg-sulphate in the low relative humidity environment of the instrument, and it is likely that much of the detected amorphous Mg-sulphate was originally crystalline. However, the paragenesis of these sulphates is unknown.

The Castile Formation evaporite on Earth is a cm-to-mm scale laminated deposit of gypsum/dolomite ($\text{CaSO}_4 \cdot 2\text{H}_2\text{O}/\text{CaMg}(\text{CO}_3)_2$) couplets that is 400–500 m thick that filled portions of the Permian basin of southeast New Mexico (~250 MYa). The deposit is thought to have formed in a shallow basin after reef growth cut off the influx of marine water, causing the basin to fill with gypsum and carbonate (Kirkland *et al.*, 2000). The carbonate–gypsum couplets are thought to represent annual changes in sedimentation, with gypsum layers forming during high evaporation (summer), and carbonate layers forming during low evaporation (winter). Some variants also include halite. Figure 8 shows X-ray mapping results from a petrologic thin section of Castile Formation evaporite, illustrating the sulphate and carbonate diurnal varves. Varves are plainly visible at both 50 μm resolution (EDAX) and 125 μm resolution (MapX-III) corresponding to alternating sulphate and carbonate layers. In the MapX ROI generated by machine learning, the varves could not be discriminated. However, the hdf5 data cube stored on the instrument is available for reprocessing and new algorithms could be devised (e.g. 'identify the locus of X, Y pixels containing Ca and Mg'), the data cube reprocessed and quantifiable XRF spectra generated from the newly calculated ROI.

Hematite/goethite diagenetic crystallization

Clastic, sand-sized particles deposited in aeolian, lacustrine, fluvial and sabkha type environments quite commonly retain their porosity and permeability after deposition. Syn-sedimentary or early diagenetic events caused by fluid migration and oxidation/reduction of soluble species can be characterized by the nature of infilling cement, precipitates, secondary crystallizations, etc. These secondary products provide a window into the pH/Eh, etc., conditions that were present when diagenetic processes were active. Figure 9, for example, shows a quartz sandstone decorated by iron oxide crystals (identified by XRD to be goethite, in all likelihood a pseudomorphic replacement of primary hematite) from Spitzbergen, Norway. The identification of secondary crystallization of Fe-oxide phases points to the early influx of soluble Fe^{++} and its oxidation and precipitation in place. Taphonomic alteration in this case would have likely destroyed evidence of the provenance of the sediment or of original habitability.

Over the course of a 10-Earth year, 30 km transect across the central mound of Gale crater (Aeolus Mons, informally known as Mt. Sharp), the MSL *Curiosity* rover has identified hundreds of examples of secondary concretions, crystals and crystal pseudomorphs in the ancient sediments of Gale lake. Knowledge of the compositions of these features will allow an evaluation of the nature of the taphonomic changes experienced by the sediments and ultimately the potential for preservation of evidence of habitability. Bristow *et al.* (2021), for example, describe Vera Rubin Ridge, an Fe-oxide rich prominent feature on lower Mt. Sharp, Gale crater, as depositionally equivalent to the immediately

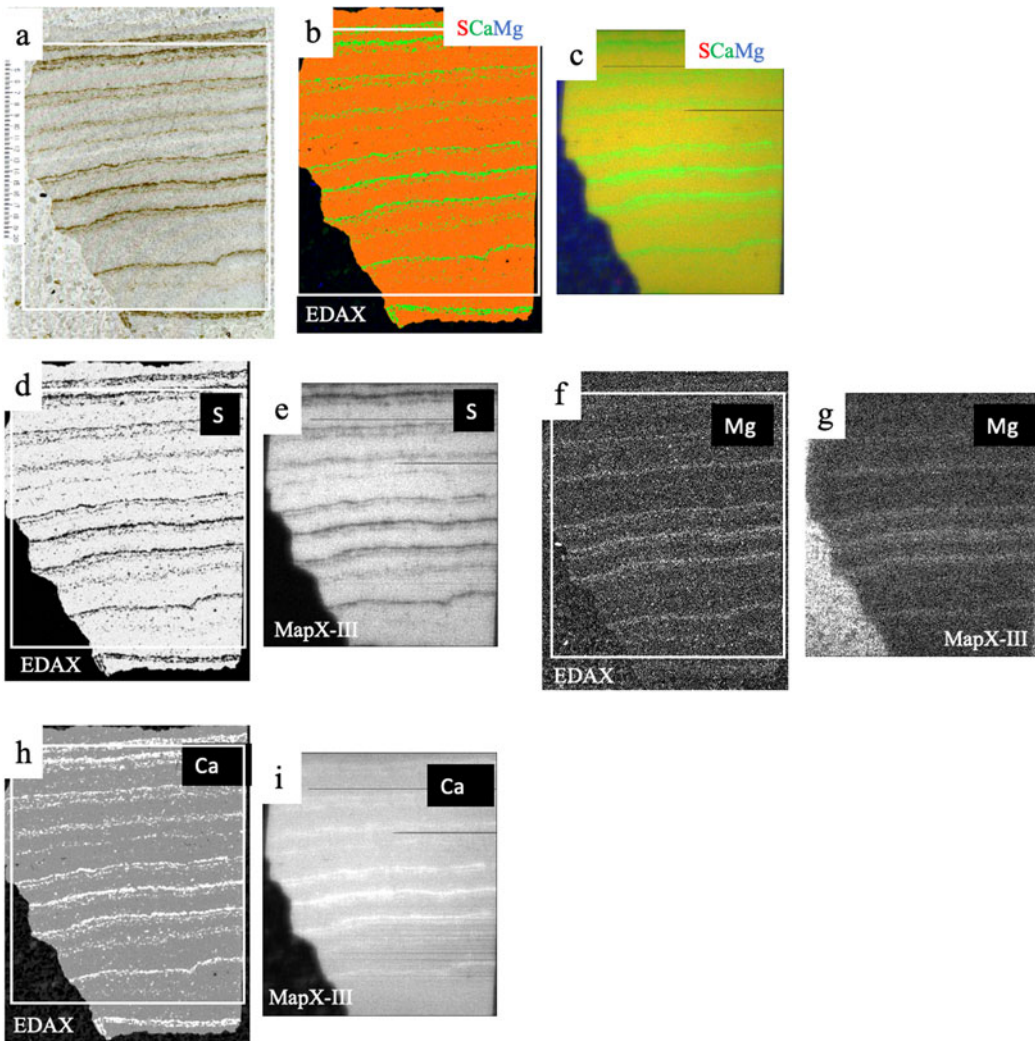


Figure 8. Castile Formation evaporite, Permian basin, New Mexico. (a) Petrographic thin section; (b) RGB element map from EDAX-Orbis instrument, Red = S, Green = Ca, Blue = Mg; (c) RGB element map from MapX-III instrument, same colour scheme as b; (d–i) comparison element images from EDAX (l) and MapX-III (r) for S, Ca and Mg (total beam power = 9 Wh (120 min analysis)).

adjacent and clay-rich Glen Torridon region. Brine-driven destruction of clay minerals caused by silica-poor diagenetic fluids is proposed as the mechanism for destruction of the original mineralogy, and under these taphonomic conditions, any evidence of habitability present in the original mudstone would likely have been erased.

Discussion

Much of what we interpret is based on images. In the case of Mars, orbital imagery prior to the arrival of the Mars Express orbiter provided information that was largely morphological in nature. Fluvial, deltaic and lacustrine features and processes were identified based on their shapes and context, analogous to similar features and processes on Earth. With orbital remote data returned from the Observatoire pour la Minéralogie, l'Eau, les Glaces et l'Activité (OMEGA) instrument

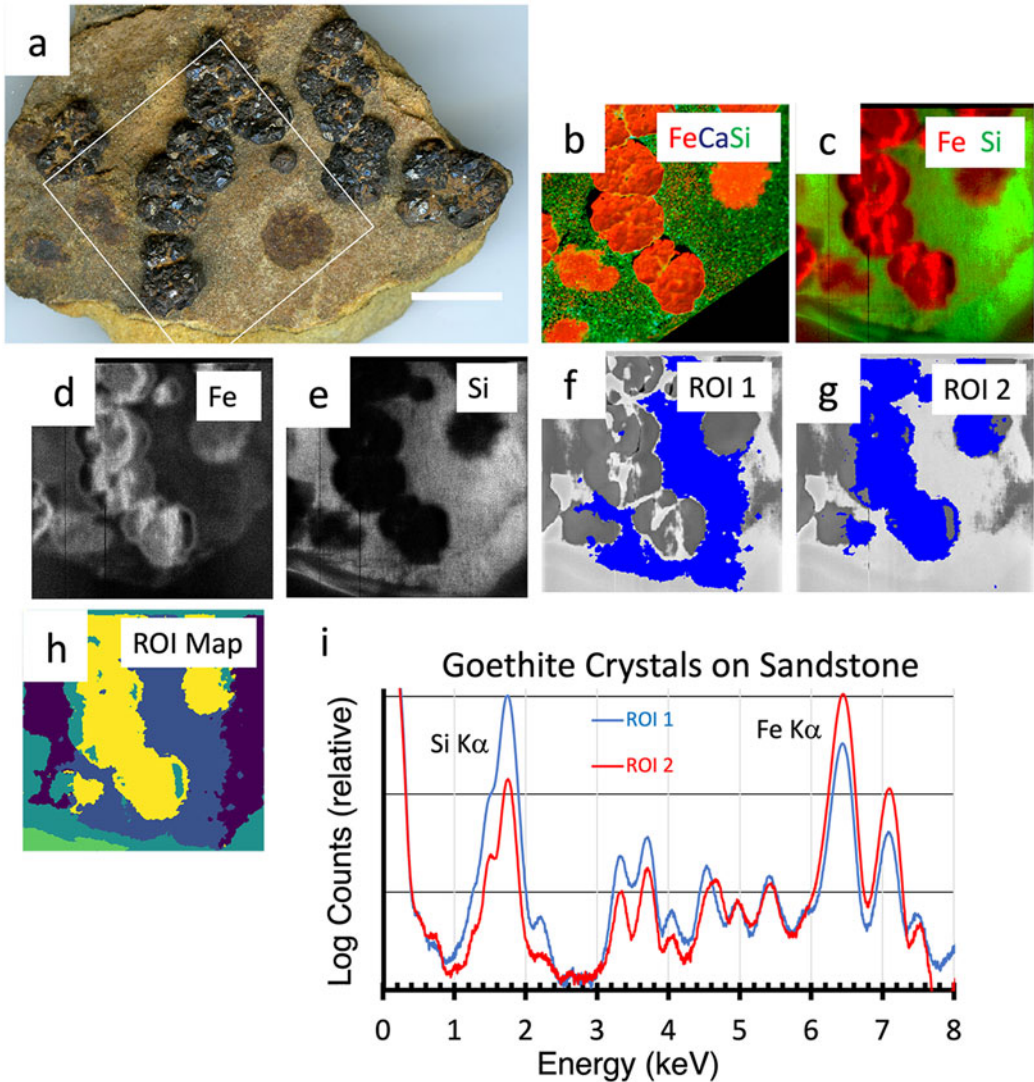


Figure 9. Goethite crystals on quartz sandstone (Spitzbergen, Norway). (a) Hand specimen, scale bar = 1 cm; (b) RGB element map from EDAX-Orbis instrument, Red = Fe, Green = Si, Blue = Ca; (c) RGB element map from MapX-III instrument, Red = Fe, Green = Si; (d) Fe map, MapX-III; (e) Si map, MapX-III; (f–h) ROI maps from MapX-III; (i) XRF spectra from ROI-1 and ROI-2, MapX-III (total beam power = 9 Wh (120 min analysis)).

on the Mars Express orbiter (Bibring *et al.*, 2005, 2006, 2007), these features could be overlain with mineralogical/compositional information, resulting in the identification of clay minerals, sulphate minerals, iron oxide minerals, etc., in spatially resolved chemical features that in many cases validated and refined earlier morphology-based interpretations. The juxtaposition of clay mineral, sulphate mineral and oxide mineral layers in sedimentary sequences on a global scale was seen to correlate with a notional understanding of the history of the planet ('Phyllosian', loosely correlated with the Noachian, 4.5–3.6 Ga; 'Theiikian', loosely correlated with the Hesperian, 3.6–2.6 Ga; and 'Siderikian', loosely correlated with the Amazonian, 2.6 Ga–present) (Bibring *et al.*, 2006; Grotzinger and Milliken, 2012).

Optical *in situ* high-resolution images of planetary regolith (e.g. from the MAHLI imagers on MER *Spirit* and *Opportunity* and MSL *Curiosity* rovers) far exceed the lateral spatial resolution of companion elemental analysis instruments such as APXS (lateral spatial resolution about 2 cm), resulting in a similar quandary: depositional and diagenetic events can be inferred from optical images, but spatially resolved elemental images are needed to fully characterize them. This has been remedied to the ~125 micron level with the development of *in situ* X-ray fluorescence imaging and the arrival of the PIXL instrument at Mars (Allwood *et al.*, 2020).

Microscale morphological information combined with elemental composition provides for a much improved interpretation of small-scale features. Principal igneous textures (flow structures, crystal fabrics) and primary sedimentary depositional fabrics (varves, ripples, etc.) can be more confidently interpreted, providing insight into modes of formation and the provenance of the source materials. Diagenetic features (concretions, secondary crystals, crystal pseudomorphs, vein fillings, alteration haloes, etc.), can be used to interpret the timing and chemistry of secondary fluids that altered rocks and primary fabrics. In returned sample science as is being initiated by Mars 2020 *Perseverance* rover, the spatially resolved elemental chemistry of features in candidate rocks is useful in evaluating samples prior to caching. Microscale chemistry informs two important questions for sample triage prior to sample return: (1) Does the original environment, as evaluated on the basis of morphology and chemistry have the potential to harbour life, and (2) Does post-depositional diagenetic change (taphonomy) preserve or destroy such features (or, did the diagenetic environment itself support habitability)?

Not surprisingly, nature doesn't obey arbitrary size constraints or specific chemistries. There is nothing unique about 125 μm resolution or even 5 μm resolution in returned images, although improvements in spatial resolution will always allow for more confident interpretations. Nearly all of the sedimentary rocks imaged during MSL *Curiosity's* traverse in Gale crater had grain sizes smaller than fine sand (<125 μm) and were in many cases below MAHLI resolution (~15 μm). Fortunately, in many cases, compositionally distinct features (element images, ROI) can be compelling if not diagnostic at spatial scales larger than the dimensions of individual mineral grains. Images of rock fabric combined with elemental chemistry tell a compelling story.

The Mars Science Laboratory rover *Curiosity* identified the first habitable environment on ancient Mars in 2013 based on the mineralogy of the ancient lake sediment found in the Sheepbed member of the Yellowknife Bay formation (Grotzinger *et al.*, 2013; Vaniman *et al.*, 2013). The presence of significant quantities of clay minerals in the John Klein and Cumberland drill samples, key to habitability, was unexpected because they were not identified in orbital spectra. This has been the case for much of *Curiosity's* transit through more than 600 vertical meters of flat-lying sedimentary rocks; clay minerals and habitable environments were found through nearly the entire traversed section despite the absence of orbital evidence for clay minerals. There are two notable exceptions: aeolian sandstones that were porous and permeable in which water was apparently never present long enough to induce diagenetic change in the original basaltic sediments, and original basaltic sediments that were diagenetically altered by late-stage fluids to the extent that evidence of habitability (or even of provenance) has been erased (e.g. Bristow *et al.*, 2021). High spatial resolution elemental images can identify and discriminate such occurrences.

Conclusions

In situ X-ray imaging instruments such as PIXL or MapX are capable of analysing the microstructure and elemental composition of rock types relevant to astrobiology rapidly and in many cases with minimal surface preparation. In searching for evidence of life or of habitable environments, the most important consideration aside from the nature of the original depositional environment is the degree of post-depositional taphonomic alteration (i.e. if evidence of life or conditions of habitability were originally present, to what extent were they preserved?). Over the past decade, MSL *Curiosity* has documented hundreds of post-depositional diagenetic features – veins, concretions,

recrystallizations, alteration halos, etc., most in the mm-size range or larger that are useful in evaluating taphonomic change.

Dozens of geologically diverse and scientifically compelling landing sites have been identified and characterized from orbit as a result of the MER, MSL and Mars 2020 site selection workshops (Grant *et al.*, 2004, 2011, 2018). In order to characterize the full geological diversity of Mars, its early habitability and its potential to support *in situ* resource utilization (ISRU) and eventual human exploration, comprehensive *in situ* science investigations need to be performed at many diverse sites. A small fleet of MER-class rovers could serve such a purpose (Blake *et al.*, 2021a), equipped with smaller, more powerful next-generation analytical instruments (e.g. Blake *et al.*, 2021b; Rampe *et al.*, 2021). If future human exploration of Mars is to be contemplated, a comprehensive understanding of the diversity of its many environments is a necessary prerequisite.

Supplementary material. The supplementary material for this article can be found at <https://doi.org/10.1017/S147355042400003X>

Data availability statement. The data that support the findings of this study are openly available in the Planetary X-ray Fluorescence Petrography database: <https://doi.org/10.48484/R7WV-3T89>

Financial support. This work was supported by awards from National Aeronautics and Space Administration (NASA) Research Opportunities in Space and Earth Science (ROSES) Planetary Instrument Concepts for the Advancement of Solar System Observations (PICASSO) program NNH13ZDA001N-PICASSO, award #13-PICASSO13-0111 and Maturation of Instruments for Solar System Exploration (MatISSE) program NNH16ZDA001N-MATISSE, award #16-MATISE16_2-0005.

Competing interest. None.

References

- Allwood AC, Wade LA, Foote MC, Elam WT, Hurrowitz JA, Battel S, Dawson DE, Denise RW, Ek EM, Gilbert MS, King, ME, Liebe CC, Parker T, Pedersen DAK, Randall DP, Sharrow RF, Sondheim ME, Allen G, Arnett K, Au MH, Basset C, Benn M, Bousman JC, Braun D, Calvet RJ, Clark B, Cinquini L, Conaby S, Conley HA, Davidoff S, Delaney JH, Denver T, Diaz E, Doran GB, Ervin J, Evans M, Flannery DO, Gao N, Gross J, Grotzinger J, Hannah B, Harris JT, Harris CM, He Y, Heirwegh CM, Hernandez C, Hertzberg E, Hodyss RP, Holden JR, Hummel C, Jadusingh C, Jorgensen JL, Kawamura JH, Kitiyakara A, Kozaczek K, Lambert JL, Lawson PR, Liu Y, Luchik T, Macneal KM, Madsen SN, McLennan SM, McNally P, Meras PL, Muller RE, Napoli J, Naylor BJ, Nemere P, Ponomarev I, Perez RM, Potraku N, Romero RA, Rosas R, Sachs J, Schaefer RT, Schein ME, Setterfield TP, Singh V, Song E, Soria MM, Stek PC, Tallarida NR, Thompson DR, Tice MM, Timmermann L, Treiman A, Tsai S, Uckert K, Villalvazo J, Wang M, Wilson DW, Worel SC, Zamani P, Zappe M, Zong F and Zimmerman R (2020) PIXL: Planetary Instrument for X-ray Lithochemistry. *Space Science Reviews* **216**, 134–268. <https://doi.org/10.1007/s11214-020-00767-7>.
- Anderson RC, Jandura L, Okon AB, Sunshine D, Roumeliotis C, Beegle LW, Hurrowitz J, Kennedy B, Limonadi D, McCloskey S, Robinson M, Seybold C and Brown K (2012) Collecting samples in Gale crater, Mars; an overview of the Mars Science Laboratory sample acquisition, sample processing and handling system. *Space Science Reviews* **170**, 57–75. <http://doi.org/10.1007/s11214-012-9898-9>.
- Awramik SM (1976) Gunflint stromatolites: microfossil distribution in relation to stromatolite morphology. In Walter MR (ed.), *Stromatolites*. Amsterdam: Elsevier, pp. 311–320.
- Barghoorn ES and Tyler SA (1965) Microorganisms from the Gunflint Chert. *Science* **147**, 563–575.
- Barnes I and O’Neil JR (1969) The relationship between fluids in some fresh alpine-type ultramafics and possible modern serpentinization, Western United States. *GSA Bulletin* **80**, 1947–1960.
- Barnes I, LaMarche Jr VC and Himmelberg G (1967) Geochemical evidence of present-day serpentinization. *Science* **156**, 830–832.
- Bibring J-P, Langevin L, Gendrin A, Gondet B, Poulet F, Berthe M, Soufflot A, Arvidson R, Mangold N, Mustard J, Drossart P, Erard S, Forni O, Combes M, Encrenaz T, Fouchet T, Merchiorri R, Belluci GC, Altieri F, Formisano F, Bonello G, Capaccioni F, Cerroni P, Coradini A, Fonti S, Kottsov V, Ignatiev N, Moroz V, Titov D, Zasova L, Pinet P, Doutes S, Schmitt B, Sotin C, Hauber E, Hoffmann H, Jaumann R, Keller U, Arvidson R, Mustard J, Duxbury T and Forget F (2005) Mars surface diversity as revealed by the OMEGA/Mars express observations. *Science* **307**, 1576–1581. <https://doi.org/10.1126/science.1108806>.
- Bibring J-P, Langevin Y, Mustard JF, Poulet F, Arvidson R, Gendrin A, Gondet B, Mangold N, Pinet P, Forget F, Berthe M, Gendrin A, Gomez C, Gondet B, Jouglet D, Poulet F, Soufflot A, Vincendon M, Combes M, Drossart P, Encrenaz T, Fouchet T, Merchiorri R, Belluci G, Alteiari F, Formisano V, Capaccioni F, Cerroni P, Coradini A, Fonti S, Korablev O, Kottsov V, Ignatiev N, Moroz V, Titov D, Zasova L, Loiseau D, Pinet P, Soute S, Schmitt B, Sotin C, Hauber E,

- Hoffmann H, Jaumann R, Keller U, Arvidson R, Mustard JF, Duxbury T and Neukum G (2006) Global mineralogical and aqueous Mars history derived from OMEGA/Mars express data. *Science* **312**, 400–404. <https://doi.org/10.1126/science.1122659>.
- Bibring J-P, Arvidson RE, Gendrin A, Gondet B, Langevin Y, Lemouelic S, Mangold N, Morris RV, Mustard JF, Poulet F, Quantin C and Sotin C (2007) Coupled ferric oxides and sulfates on the Martian surface. *Science* **317**, 1206–1210. <https://doi.org/10.1126/science.1144174>.
- Bish DL, Blake DF, Vaniman DT, Chipera SJ, Morris RV, Ming DW, Treiman AH, Sarrazin P, Morrison SM, Downs RT, Achilles CN, Yen AS, Bristow TF, Crisp JA, Rampe EB, Stolper EM, Spanovich N and Morookian JM (2013) X-ray diffraction results from Mars Science Laboratory: mineralogy of Rocknest aeolian bedform at Gale crater. *Science* **341**, 1238932. <https://doi.org/10.1126/science.1238932>.
- Bishop JL, Parente M, Weitz CM, Noe Dobrea EZ, Roach LH, Murchie SL, McGuire PC, McKeown NK, Rossi CM, Brown AJ, Calvin WM, Milliken R and Mustard JF (2009) Mineralogy of Juventae Chasma: sulfates in the light-toned mounds, mafic minerals in the bedrock, and hydrated silica and hydroxylated ferric sulfate on the plateau. *Journal of Geophysical Research* **114**, E00D09. <https://doi.org/10.1029/2009JE003352>.
- Blake DF and Peacor DR (1985) TEM/STEM microanalysis of Holocene fresh-water Magnesian carbonate cements from the coast range of California. *American Mineralogist* **70**, 388–394.
- Blake DF, Treiman AH, Morris R, Bish D, Amundsen HEF and Steele A (2011) ‘Carbonate cements from the Sverrefjell and Sigurd fjell Volcanoes, Svalbard, Norway: analogs for Martian carbonates.’ *LPSC 42*, The Woodlands, TX, March 7–11, 2011. Abstr. #2167, Available at <https://www.lpi.usra.edu/meetings/lpsc2011/pdf/2167.pdf>
- Blake DF, Sarrazin P and Bristow T (2015) ‘Mapping X-ray Fluorescence Spectrometer (Map-X).’ *LPSC 46*, The Woodlands, TX, March 16–20, 2015. Abstr. #2274. Available at <https://www.hou.usra.edu/meetings/lpsc2015/pdf/2274.pdf>
- Blake DF, Walroth R, Bristow T, Sarrazin P, Gailhanou M, Downs R and Thompson K (2021a) MapX: an in-situ X-ray μ -mapper for habitability and biosignature studies. *Bulletin of the American Astronomical Society* **53**, 1–5. <https://doi.org/10.3847/25c2cfcb.d0806478>.
- Blake DF, Zacny K, Bristow T, Morrison S, Sarrazin P, Rampe E, Tu V, Thorpe MT, Payre V, Smith R, Scudder N, Bedford CC and Dehouck E (2021b) MER-class rover investigations of Mars in the coming decades. *Bulletin of the American Astronomical Society* **53**, 1–5. <https://doi.org/10.3847/25c2cfcb.a7226c13>.
- Blake DF, Vaniman D, Achilles C, Anderson R, Bish D, Bristow T, Chen C, Chipera S, Crisp J, Des Marais DJ, Downs RT, Farmer J, Feldman S, Fonda M, Gailhanou M, Ma H, Ming DW, Morris RV, Sarrazin P, Stolper E, Treiman A and Yen A (2012) Characterization and calibration of the CheMin mineralogical instrument on Mars Science Laboratory. *Space Science Reviews* **170**, 57–75.
- Blake DF, Morris RV, Kocurek G, Morrison SM, Downs RT, Bish DL, Ming DW, Edgett KS, Rubin D, Goetz W, Madsen MB, Sullivan R, Gellert R, Campbell I, Treiman AH, McClennan SM, Yen AS, Grotzinger J, Vaniman DT, Chipera SJ, Achilles CN, Rampe EB, Sumner D, Navsline P-Y, Maurice S, Forni O, Gasnault O, Fisk M, Schmidt M, Mahaffy P, Leshin LA, Glavin D, Steele A, Freissinet C, Navarro-Gonzalez R, Yingst RA, Kah LC, Bridges N, Lewis KW, Bristow TF, Farmer JD, Crisp JA, Stolper EM, Des Marais DJ and Sarrazin P and the Mars Science Laboratory Science Team (2013) Curiosity at Gale crater, Mars: characterization and analysis of the Rocknest sand shadow. *Science* **341**, 1239505.
- Bridges JC and Grady MM (2000) Evaporite mineral assemblages in the Nakhilite (Martian) meteorites. *Earth and Planetary Science Letters* **176**, 267–279. [https://doi.org/10.1016/S0012-821X\(00\)00019-4](https://doi.org/10.1016/S0012-821X(00)00019-4).
- Bridges JC and Schwenzer SP (2012) The Nakhilite hydrothermal brine on Mars. *Earth and Planetary Science Letters* **359–360**, 117–123. [https://doi.org/10.1016/S0012-821X\(00\)00019-4](https://doi.org/10.1016/S0012-821X(00)00019-4).
- Bridges JC, Hicks LJ and Treiman AH (2018) Carbonates on Mars. In Filiberto J and Schwenzer SP (eds), *Volatiles in the Martian Crust*. Elsevier, pp. 89–118. <http://dx.doi.org/10.1016/B978-0-12-804191-8.00005-2>.
- Bristow TF, Bish DL, Vaniman DT, Morris RV, Blake DF, Grotzinger JP, Rampe EB, Crisp JA, Achilles CN, Ming DW, Ehlmann DL, King PL, Bridges JC, Eigenbrode JL, Sumner DY, Chipera J, Moorokian JM, Treiman AH, Morrison SM, Downs RT, Farmer JD, Des Marais DJ, Sarrazin P, Floyd MM, Mishna MA and McAdam AC (2015) The origin and implications of clay minerals from Yellowknife Bay, Gale crater, Mars. *American Mineralogist* **100**, 824–836. <https://doi.org/10.2138/am-2015-5077CCBYNCND>.
- Bristow TF, Grotzinger JP, Rampe EB, Cuadros J, Chipera SJ, Downs GW, Fedo CM, Frydenvang J, McAdam AC, Morris RV, Achilles CN, Blake DF, Castle N, Craig P, Des Marais DJ, Downs RT, Hazen RM, Ming DW, Morrison SM, Thorpe MT, Treiman AH, Tu V, Vaniman DT, Yen AS, Gellert R, Mahaffy PR, Wiens RC, Byrk AB, Bennett KA, Fox VK, Milliken RE, Fraeman AA and Vasavada AR (2021) Brine-driven destruction of clay minerals in Gale crater, Mars. *Science* **373**, 198–204. <https://doi.org/10.1126/science.abg5449>.
- Campbell JL, Perrett GM, Gellert R, Andrusenko SM, Boyd NI, Maxwell JA, King PL and Schofield CD (2012) Calibration of the Mars Science Laboratory Alpha Particle X-ray Spectrometer. *Space Science Reviews* **170**, 319–340. <https://doi.org/10.1007/s11214-012-9873-5>.
- Chipera SJ, Vaniman DT, Rampe EB, Bristow TF, Martinez G, Tu VM, Peretyazhko TS, Yen AS, Gellert R, Berger JA, Rapin W, Morris RV, DW, Thompson LM, Simpson S, Achilles CN, Tutolo B, Downs RT, Fraeman AA, Fischer E, Blake DF, Treiman AH, Morrison SM, Thorpe MT, Gupta S, Dietrich WE, Downs G, Castle N, Craig PI, Des Marais DJ, Hazen RM, Vasavada AR, Hausrath E, Sarrazin P and Grotzinger JP (2023) Mineralogical investigation of Mg-sulfate at the Canaima drill site, Gale crater, Mars. *Journal of Geophysical Research: Planets* **128**, 1–16. <https://doi.org/10.1029/2023JE008041>.

- Christensen PR, Mehall GL, Silverman SH, Anwar S, Cannon G, Gorelick N, Kheen R, Tourville T, Bates D, Ferry S, Fortuna T, Jeffreys J, O'Donnell W, Peralta R, Wolverton T, Blaney D, Denise R, Radermacher J, Morris RV and Squyres S (2003) Miniature Thermal Emission Spectrometer for the Mars Exploration Rovers. *Journal of Geophysical Research: Planets* **108**, 8064. <https://doi.org/10.1029/2003JE002117>.
- Coleman RG (2000) 'Prospecting for ophiolites along the California Continental Margin.' In *Ophiolites and Oceanic Crust: New Insights from Field Studies and the Ocean Drilling Program*, Geological Society of America Special Paper 349, edited by Y. Dilek, E. Moores, D. Elthon, and A. Nicolas, Geological Society of America, Boulder, CO, pp. 351–364.
- Deming JW and Baross JA (1993) Deep-sea smokers: windows to a subsurface biosphere? *Geochimica et Cosmochimica Acta* **57**, 3219–3230. [http://doi.org/10.1016/0016-7073\(93\)90535-5](http://doi.org/10.1016/0016-7073(93)90535-5).
- Economou TE (2011) History of applications of radioactive sources in analytical instruments for planetary exploration. In Singh N (ed.), *Radioisotopes: Applications in Physical Sciences*. InTech, pp. 155–172. <http://dx.doi.org/10.5772/23087>.
- Edgett KS, Yingst RA, Ravine MA, Caplinger MA, Ghaemi FT, Maki JN, Schaffner JA, Bell JF, Edwards LJ, Herkenhoff KE and Heydari E (2012) Curiosity's Mars Hand Lens Imager (MAHLI) investigation. *Space Science Reviews* **170**, 259–317. <https://doi.org/10.1007/s11214-012-9910-4>.
- Ehlmann BL and Edwards CS (2014) Mineralogy of the Martian surface. *Annual Review of Earth and Planetary Sciences* **42**, 291–315. <https://doi.org/10.1146/annurev-earth-060313-055024>.
- Ehlmann BL, Mustard JF, Murchie SL, Poulet F, Bishop JL, Brown AJ, Calvin WM, Clark RN, Des Marais DJ, Milliken RE, Roach LH, Rousch TL, Swayze GA and Wray JJ (2008) Orbital identification of carbonate-bearing rocks on Mars. *Science* **322**, 1828–1832. <http://doi.org/10.1126/science.1164759>.
- Farley KA, Stack KM, Shuster DL, Horgan BHN, Hurowitz JA, Tarnas JD, Simon JI, Sun VZ, Scheller EL, Moore KR, McLennan SM, Vasconcelos PM, Wiens RC, Treiman AH, Mayhew LE and the Mars 2020 Science Team (2022) Aqueously altered igneous rocks sampled on the floor of Jezero crater, Mars. *Science* **377**, 1–11. <https://doi.org/10.1126/science.abo2196>.
- Fraser GW, Carpenter JD, Rothery DA, Pearson JF, Martindale A, Huovelin J, Treis J, Anand M, Anttila M, Ashcroft M, Benkoff J, Bland P, Bowyer A, Bradley A, Bridges J, Brown C, Bullock C, Bunce EJ, Christensen U, Evans M and Whitehead S (2010) The Mercury Imaging X-ray Spectrometer (MIXS) on Bepicolombo. *Planetary and Space Science* **58**, 79–95. <https://doi.org/10.1016/j.pss.2009.05.004>.
- Gailhanou M, Sarrazin P and Blake DF (2018) Modeling of X-ray fluorescence full field imaging using planar square pore micro-channel plate optics. *Journal Applied Optics* **57**, 6795–6807. <https://doi.org/10.1364/AO.57.006795>.
- Gellert R, Rieder R, Bruckner J, Clark BC, Dreibus G, Klingelhofer G, Lugmair G, Ming DW, Wanke H, Yen A, Zipfel J and Squyres SW (2006) Alpha Particle X-ray Spectrometer (APXS): results from Gusev crater and calibration report. *Journal of Geophysical Research* **111**, 1–32. <https://doi.org/10.1029/2005JE002555>.
- Grant JA, Golombek MP, Parker TJ, Crisp JA, Squyres SW and Weitz CM (2004) Selecting landing sites for the 2003 Mars Exploration Rovers. *Planetary and Space Science* **52**, 11–21. <http://doi.org/10.1016/j.pss.2003.08.011>.
- Grant JA, Golombek MP, Grotzinger JP, Wilson SA, Watkins MM, Vasavada AR, Griffes JL and Parker TJ (2011) The science process for selecting the landing site for the 2011 Mars Science Laboratory. *Planetary and Space Science* **59**, 1114–1127. <https://doi.org/10.1016/j.pss.2010.06.016>.
- Grant JA, Golombek MP, Wilson SA, Farley KA, Williford KH and Chen A (2018) The science process for selecting the landing site for the 2020 Mars rover. *Planetary and Space Science* **164**, 106–126. <https://doi.org/10.1016/j.pss.2018.07.001>.
- Grotzinger JP and Milliken RE (2012) The sedimentary rock record of Mars: distribution, origins and global stratigraphy. In Grotzinger JP and Milliken RE (eds), *Sedimentary Geology of Mars*. <https://doi.org/10.2110/pec.12.102.0001>
- Grotzinger JP, Crisp J, Vasavada AR, Anderson RC, Baker CJ, Barry R, Blake DF, Conrad P, Edgett KS, Ferdowski B, Gellert R, Gilbert JB, Golombek M, Gomez-Elvira J, Hassler DM, Jandura L, Litvac M, Mahaffy P, Maki J, Meyer M, Mitrofanov I, Simonds JL, Vaniman D, Welch RV and Wiens RC (2012) Mars Science Laboratory mission and science investigation. *Space Science Reviews* **170**, 57–75. <https://doi.org/10.1007/s11214-012-9892-2>.
- Grotzinger JP, Sumner DY, Kah LC, Stack K, Gupta S, Edgar L, Rubin D, Lewis K, Schieber J, Mangold N, Milliken R, Conrad D, Des Marais D, Farmer J, Siebach K, Calef III F, Hurowitz J, McLennan SM, Ming D, Vaniman D, Crisp J, Vasavada A, Edgett KS, Malin M, Blake D, Gellert R, Mahaffy P, Wiens RC, Maurice S, Grant J and the Mars Science Laboratory Science Team (2013) A habitable Fluvio-lacustrine environment at Yellowknife Bay, Gale crater, Mars. *Science* **343**, 1242777. <https://doi.org/10.1126/science.1242777>
- Herkenhoff KE, Squyres SW, Bell III JF, Maki JN, Arneson HM, Bertelsen P, Brown DI, Collins SA, Dingizian A, Elliott ST, Goetz W, Hagerott EC, Hayes AG, Johnson MJ, Kirk RL, McLennan S, Morris RV, Scherr LM, Schwochert MA, Shiraishi LR, Smith GH, Soderblom LA, Sohl-Dickstein JM and Wadsworth MV (2003) Athena Microscopic Imager investigation. *Journal of Geophysical Research: Planets* **108**, 8065. <https://doi.org/10.1029/2003JE002076>.
- Herkenhoff KE, Grotzinger J, Knoll AH, McLennan SM, Weitz C, Yingst A, Anderson R, Archinal BA, Arvidson RE, Barrett JM, Becker KJ, Bell III JF, Budney C, Chapman MG, Cook D, Ehlmann B, Franklin B, Gadis LR, Galuszka DM, Garcia PA, Geissler P, Hare TM, Howington-Krause E, Johnson JR, Keszthelyi L, Kirk RL, Lanagan P, Lee EM, Leiff C, Maki JN, Mullins KF, Parker TJ, Redding BL, Roseik MR, Sims MH, Soderblom LA, Spanovich N, Springer R, Squyres SW, Stolper D, Sucharski RM, Tucharski T, Sullivan R and Torson JM (2008) Surface processes recorded by rocks and soils on Meridiani Planum, Mars: microscopic imager observations during Opportunity's first three extended missions. *Journal of Geophysical Research* **113**, 1–39. <https://doi.org/10.1029/2008JE003100>.

- Hickman-Lewis K, Moore KR, Razzell-Hollis JJ, Tuite ML, Beegle LM, Bhartia R, Grotzinger JP, Brown AJ, Shkolyar S, Cavalazzi B and Smith CL (2022) *In situ* identification of paleoarchean biosignatures using colocated Perseverance rover analyses: perspectives for *in situ* Mars science and sample return. *Astrobiology* **22**, 1143–1163. <https://doi.org/10.1089/ast.2022.0018>.
- Kelley DS, Karson JA, Blackman DK, Fruh-Green GL, Butterfield DA, Lilley MD, Olson EJ, Schrenk MO, Roe KK, Lebon GT and Rivizzigno P, (2001a) An off-axis hydrothermal vent field near the mid-Atlantic ridge at 30°N. *Nature* **412**, 145–149. <https://doi.org/10.1038/35084000>.
- Kelley D, Karson J, Blackman D, Fruh-Green G, Butterfield D, Lilley M, Schrenk M, Olson E, Roe K and Lebon J (2001b) Discovery of lost city: an off-axis, peridotite hosted, hydrothermal field near 30°N on the mid-Atlantic ridge. *Ridge Events* **11**, 3–9.
- Kelley DS, Karson JA, Fruh-Green GL, Yoerger DR, Shank TM, Butterfield DA, Hayes JM, Schrenk MO, Olson EJ, Proskurowski G, Jakuba M, Bradley A, Larson B, Ludwig K, Glickson D, Buckman K, Bradley AS, Brazelton WJ, Roe K, Elend MJ, Delacour A, Bernasconi SM, Lilley MD, Baross JA, Summons RE and Sylvia SP (2005) A serpentinite-hosted ecosystem: the lost city hydrothermal field. *Science* **307**, 1428–1434. <https://doi.org/10.1126/science.1102556>.
- Kirkland DW, Dennison RE and Dean WE (2000) Parent brine of the Castile evaporites (Upper Permian), Texas and New Mexico. *Journal of Sedimentary Research* **70**, 749–761. <https://doi.org/10.1306/2dc40935-0e47-11d7-8643000102c1865d>.
- Knoll AH (1985) Exceptional preservation of photosynthetic organisms in silicified carbonates and silicified peats. *Philosophical Transactions of the Royal Society B* **311**, 111–122.
- Lafuente B, Downs RT, Yang H and Stone N (2015) The power of databases: the RRUFF project. In Armbruster T and Danisi RM (eds). *Highlights in Mineralogical Crystallography*. Berlin, Germany: W. DeGruyter, pp. 11–30. <https://doi.org/10.1515/9783110417104-003>.
- Liu Y, Tice MM, Schmidt ME, Treiman AH, Kizovski TV, Hurowitz JA, Allwood AC, Henneke J, Pedersen DAK, VanBommel SJ, Jones MWM, Knight AL, Orenstein BJ, Clark BC, Elam WT, Heirwegh CM, Barber T, Beegle LW, Benzerara K, Bernard S, Beyssac O, Bosak T, Brown AJ, Cardarelli EL, Catling DC, Christian JR, Cloutis EA, Cohen BA, Davidoff S, Fairen AG, Farley KA, Flannery DT, Galvin A, Grotzinger JP, Gupta S, Hall J, Herd CDK, Hickman-Lewis K, Hodyss RP, Horgan BHN, Johnson JR, Jorgensen JL, Kah LC, Maki JN, Mandon L, Mangold N, McCubbin FM, McLennan SM, Moore K, Nachon M, Nemere P, Nothdurft LD, Nunez JI, O’Neil L, Quantin-Nataf CM, Sautier V, Shuster DL, Siebach KL, Simon JI, Sinclair KP, Stack KM, Steele A, Tarnas JD, Tosca NJ, Uckert K, Udry A, Wade LA, Weiss BP, Wiens RC, Williford KH and Zorzano M-P (2022) An olivine cumulate outcrop on the floor of Jezero crater, Mars. *Science* **377**, 1513–1519. <https://doi.org/10.1126/science.abo2757>.
- Mahaffy PR, Webster CR, Cabane M, Conrad PG, Coll P, Atreya SK, Arvey R, Barciniak M, Benna M, Bleacher L, Brinkerhoff WB, Eigenbrode JL, Carignan D, Cascia M, Chalmers RA, Dworkin JP, Errigo T, Everson P, Franz H, Farley R, Feng S, Frazier G, Freissinet C, Glavin DP, Harpold DN, Hawk D, Holmes V, Johnson CS, Jones A, Jordan P, Kellogg J, Lewis J, Lyness E, Malespin CA, Martin DK, Maurer J, McAdam AC, McLennan D, Nolan TJ, Noriega M, Pavlov AA, Prats B, Raaen E, Sheinman O, Sheppard D, Smith J, Stern JC, Tan F, Trainer M, Ming DW, Morris RV, Jones J, Gunderson C, Steele A, Wray J, Botta O, Leshin LA, Owen T, Battel S, Jakosky BM, Manning H, Squyres S, Navarro-Gonzalez R, McKay CP, Raulin F, Sternberg R, Buch A, Sorensen P, Kline-Schoder R, Coscia D, Szopa C, Teinturier S, Baffes C, Feldman J, Flesch G, Forouhar S, Garcia R, Keymeulen D, Woodward S, Block BP, Arnet K, Miller R, Edmonson C, Gorevan S and Mumm E (2012) The sample analysis at Mars investigation and instrument suite. *Space Science Reviews* **170**, 401–478. <https://doi.org/10.1007/s11214-012-9879-z>.
- Maurice S, Wiens RC, Saccoccio M, Barraclough B, Gasnault O, Forni O, Mangold N, Baratoux D, Bender S, Berger G, Bernadin J, Berthe M, Bridges N, Blaney D, Bouye M, Cais P, Clark B, Clegg S, Cousin A, Cremers D, Cros A, DeFlores L, Derycke C, Dingler B, Dromart G, Dubois B, Dupieux M, Durand E, d’Uston L, Fabre C, Faure B, Gaboriaud A, Gharsa T, Herkenhoff K, Kan E, Kirkland L, Kouach D, Lacour J-L, Langevin Y, Lasue J, LeMouelic S, Lescure M, Lewin E, Limonadi D, Manhes G, Mauchien P, McKay C, Meslin P-Y, Michel Y, Miller E, Newsom HE, Ortner G, Paillet A, Pares aL, Parot Y, Perez R, Pinet P, Poitrasson F, Quartier B, Salle B, Sotin C, Sautter V, Seran H, Simmonds JJ, Sirven J-B, Stiglich R, Striebig N, Thocaven J-J, Toplis MJ and Vaniman D (2012) The ChemCam instrument suite on the Mars Science Laboratory (MSL) rover: science objectives and mast unit description. *Space Science Reviews* **170**, 95–166. <https://doi.org/10.1007/s11214-012-9912-2>.
- McCollom TM and Shock EL (1997) Geochemical constraints on chemolithoautotrophic metabolism by microorganisms in sea-floor hydrothermal systems. *Geochimica et Cosmochimica Acta* **61**, 4375–4391. [https://doi.org/10.1016/S0016-7037\(97\)00241-X](https://doi.org/10.1016/S0016-7037(97)00241-X).
- McKay DS, Gibson Jr EK, Thomas-Keptra KL, Vali H, Romanek CS, Clemett SJ, Chillier XD, Maechling CR and Zare RN (1996) Search for past life on Mars: possible relict biogenic activity in Martian meteorite ALH84001. *Science* **273**, 924–930. <https://doi.org/10.1126/science.273.5277.924>.
- McLennan SM (2003) Sedimentary silica on Mars. *Geology* **31**, 15–318. [https://doi.org/10.1130/0091-7613\(2003\)031<0315:SSOM>2.0.CO;2](https://doi.org/10.1130/0091-7613(2003)031<0315:SSOM>2.0.CO;2).
- McLennan SM, Bell III JF, Calvin WM, Christensen PR, Clark BC, de Souza PA, Farmer J, Farrand WH, Fike DA, Gellert R, Gosh A, Glotch TD, Grotzinger JP, Hahn B, Herkenhoff KE, Hurowitz JA, Johnson JR, Johnson SS, Joliff B, Klingelhofer G, Knoll AH, Learner Z, Malin MC, McSween Jr HY, Pockock J, Ruff SW, Soderblom LA, Squyres SW, Tosca NJ, Watters WA,

- Wyatt MB and Yen A (2005) Provenance and diagenesis of the evaporite bearing burns formation, Meridiani Planum, Mars. *Earth and Planetary Science Letters* **240**, 95–121. <http://doi.org/10.1016/j.epsl.2005.09.041>.
- Milliken RE, Swayze GA, Arvidson RE, Bishop JL, Clark RN, Ehlmann BL, Green RO, Grotzinger JP, Morris RV, Murchie SL, Mustard JF and Weitz C (2008) Opaline silica in young deposits on Mars. *Geology* **36**, 847–850. <http://doi.org/10.1130/G24967A.1>.
- Milliken RE, Grotzinger JP and Thomson BJ (2010) Paleoclimate of Mars as captured by the stratigraphic record in Gale crater. *Geophysical Research Letters* **37**, L04201. <https://doi.org/10.1029/2009GL041870>.
- Morris RV, Klingelhofer G, Schroder C, Rodionov DS, Yen A, Ming DW, de Souza Jr PA, Fleischer I, Wdowiak T, Gellert R, Bernhardt B, Evlanov EN, Zubkov B, Foh J, Bonnes U, Kankleit E, Gutlich P, Renz F, Squyres SW and Arvidson RE (2006) Mössbauer mineralogy of rock, soil, and dust at Gusev crater, Mars: Spirit's journey through weakly altered olivine basalt on the plains and pervasively altered basalt in the Columbia Hills. *Journal of Geophysical Research* **111**, E02S13. <http://doi.org/10.1029/2005JE002584>.
- Morris RV, Ruff SW, Gellert R, Ming DW, Arvidson RE, Clark BC, Golden DC, Siebach K, Klingelhofer G, Schroder C, Fleischer I, Yen A and Squyres SW (2010) Identification of carbonate-rich outcrops on Mars by the Spirit rover. *Science* **29**, 421–424. <https://doi.org/10.1126/science.1189667>.
- Morris RV, Blake DF, Bish D, Ming DW, Agresti DG, Treiman AH, Steele A and Amundsen HEF (2011) 'A terrestrial analogue from Spitsbergen (Svalbard, Norway) for the Comanche Carbonate at Gusev Crater, Mars.' *LPSC 42*, Abstract # 1699. Available at <https://www.lpi.usra.edu/meetings/lpsc2011/pdf/1699.pdf>.
- Morris RV, Vaniman DT, Blake DF, Gellert R, Chipera SJ, Rampe EB, Ming DW, Morrison SM, Downs RT, Treiman AH, Yen AS, Grotzinger JP, Achilles CN, Bristow TF, Crisp JA, Des Marais DJ, Farmer JD, Fendich KV, Frydenvang J, Graff TG, Morookian JM, Stolper EM and Schwenzer SP (2016) Silicic volcanism on Mars evidenced by Tridymite in high-SiO₂ sedimentary rock at Gale crater. *Proceedings of the National Academy of Sciences of the USA* **113**, 7071–7076. <https://doi.org/10.1073/pnas.1607098113>.
- Pia MG, Weidenspointer G, Augelli M, Quintieri L, Saracco P, Sudhakar M and Zoglauer A (2009) PIXE simulation with Geant4. *IEEE Transactions on Nuclear Science* **56**, 3614–3649. <https://doi.org/10.1109/TNS.2009.2033993>.
- Price GJ, Fraser GW, Pearson JF, Nussey JP, Hutchinson IB, Holland AD, Turner K and Pullan P (2004) Prototype imaging X-ray fluorescence spectrometer based on microchannel plate optics. *Review of Scientific Instruments* **75**, 2314–2319. <http://doi.org/10.1063/1.764610>.
- Rampe EB, Ming DW, Blake DF, Bristow TF, Chipera SJ, Grotzinger JP, Morris RV, Morrison SM, Vaniman DT, Yen AS, Achilles CN, Craig PI, Des Marais DJ, Downs RT, Farmer JD, Fendrich KV, Gellert R, Morookian JM, Peretyazhko TS, Sarrazin P, Treiman AH, Berger JA, Eigenbrode JL, Fairen AG, Forni O, Gupta S, Hurowitz JA, Kah LC, Lanza NL, Schmidt ME, Siebach K, Sutter B and Thompson LC (2017) Mineralogy of an ancient lacustrine mudstone succession from the Murray formation, Gale crater, Mars. *Earth and Planetary Science Letters* **471**, 172–185. <http://doi.org/10.1016/j.epsl.2017.04.021>.
- Rampe EB, Blake D, Sarrazin P, Bristow T, Gailhanou M, Lafuente B, Tu V, Zacny K and Downs R (2021) CheMinX: a next generation XRD/XRF for quantitative mineralogy and geochemistry on Mars. *Bulletin of the American Astronomical Society* **53**. <https://doi.org/10.3847/25c2cfcb.a4a55445>
- Razzell HJ, Moore KR, Sharma S, Beegle L, Grotzinger JP, Allwood A, Abbey W, Bharita R, Brown AJ, Clark B, Cloutis E, Corpolongo A, Henneke J, Hickman-Lewis K, Hurowitz J, Jones MWM, Liu Y, Martinez-Frias J, Murphy A, Pedersen DAK, Shkoliar S, Siljestrom S, Steele A, Tice M, Treiman A, Uckert K, VanBommel S and Yanchilina A (2022) The power of paired proximity science observations: co-located data from SHERLOC and PIXL on Mars. *Icarus* **387**, 115179. <http://doi.org/10.1016/j.icarus.2022.115179>.
- Rieder R, Gellert R, Bruckner J, Klingelhofer G, Dreibus G, Yen A and Squyres SW (2003) The new Athena Alpha Particle X-ray Spectrometer for the Mars Exploration Rovers. *Journal of Geophysical Research: Planets* **108**, 8066. <https://doi.org/10.1029/2003JE002150>.
- Ruff SW, Christensen PR, Blaney DL, Farrand WH, Johnson JR, Michaelski JR, Moersch JE, Wright SP and Squyres SW (2006) The rocks of Gusev crater as viewed by the Mini-TES instrument. *Journal of Geophysical Research* **111**, E12S18. <https://doi.org/10.1029/2006JE002747>.
- Sarrazin P, Blake D, Thompson K, Gailhanou M, Chen J and Bristow T (2016) 'The Map-X μ -imaging XRF spectrometer.' *LPSC 47*, The Woodlands, TX, March 21–25, 2016. Abstr. #2883, Available at <https://www.hou.usra.edu/meetings/lpsc2016/pdf/2883.pdf>
- Sarrazin P, Blake D, Gailhanou M, Marchis F, Chalumeau C, Webb S, Walter P, Schyns E, Thompson K and Bristow T (2018) MapX: 2D XRF for planetary exploration – image formation and optic characterization. *Journal of Instrumentation* **13**, C04023. <https://doi.org/10.1088/1748-0221/13/04/C04023>.
- Scheller EL, Hollis JR, Cardarelli EL, Steele A, Beegle L, Bharita R, Conrad P, Uckert K, Sharma S, Ehlmann BL, Abbey WJ, Asher SA, Benison KC, Berger EL, Beyssac O, Bleefeld BL, Bosak T, Brown AJ (2023) Aqueous alteration processes in Jezero crater, Mars – implications for organic geochemistry. *Science* **378**, 1105–1110. <https://doi.org/10.1126/science.abo5204>.
- Schoonjans T, Brunetti A, Golosio B, del Rio MS, Sole VA, Ferrero C and Vincze L (2012) The Xraylib library for X-ray – matter interactions. Recent developments. *Spectrochimica Acta Part B* **70**, 10–23. <https://doi.org/10.1016/j.sab.2011.09.011>.

- Schulte M, Blake D, Hoehler T and McCollom T (2006) Serpentinization and its implications for life on the early Earth and Mars. *Journal of Astrobiology* **6**, 364–376. <https://doi.org/10.1089/ast.2006.6.364>.
- Sepúlveda M, Pozzi-Escot D, Falcon RA, Bermeo N, Lebon M, Moulherat C, Sarrazin P and Walter P (2020) Unraveling the polychromy and antiquity of the Pachacamac Idol, Pacific Coast, Peru. *PLoS ONE* **15**, e0226244. <https://doi.org/10.1371/journal.pone.0226244>.
- Sleep NH, Meibom A, Fridriksson T, Coleman RG and Bird DK (2004) H₂-rich fluids from serpentinization: geochemical and biotic implications. *Proceedings of the National Academy of Sciences of the USA* **101**, 12818–12823. <https://doi.org/10.1073/pnas.0405289101>.
- Solé VA, Papillon E, Cotte M, Walter P and Susini J (2007) A multiplatform code for the analysis of energy-dispersive X-ray fluorescence spectra. *Spectrochimica Acta Part B* **62**, 63–68. <https://doi.org/10.1016/j.sab.2006.12.002>.
- Squyres SW, Grotzinger JP, Arvidson RE, Bell III JF, Calvin W, Christensen PR, Farrand WH, Herkenhoff KE, Johnson JR, Klingelhofer G, Knoll A, McLennan SM, McSween HY, Morris RV, Rice Jr JW, Rieder R and Soderblom LA (2006) *In situ* evidence for an ancient aqueous environment at Meridiani Planum, Mars. *Science* **06**, 1709–1714. <https://doi.org/10.1126/science.1104559>.
- Squyres SW, Arvidson RE, Ruff S, Gellert R, Morris RV, Ming DW, Crumpler L, Farmer JD, Des Marais DJ, Yen A, McClennan SM, Calvin W, Bell III JF, Clark BC, Wang A, McCoy TJ, Schmidt ME and DeSouza Jr PA (2008) Detection of silica-rich deposits on Mars. *Science* **320**, 1063–1067. <https://doi.org/10.1126/science.1155429>.
- Thompson KA, Blake DF and Sarrazin P (2017) ‘X-ray fluorescence source modeling for the MapX imaging spectrometer: rocky planets and ocean worlds.’ LPSC 48, The Woodlands, TX, March 20–24, 2017. Abstr. #1602, Available at <https://www.hou.usra.edu/meetings/lpsc2017/pdf/1602.pdf>
- Tice MM, Hurowitz JA, Allwood AC, Jones MWM, Orenstein BJ, Davidoff S, Wright AP, Pedersen DAK, Henneke J, Tosca NJ, Moore KR, Clark BC, McLennan SM, Flannery DT, Steele A, Brown AJ, Zorzano M-P, Hickman-Lewis K, Liu Y, VanBommel SJ, Schmidt ME, Kizovski TV, Treiman AH, O’Neil L, Fairen AG, Shuster DL and Gupta S (2022) Alteration history of Seitah formation rocks inferred by PIXL X-ray fluorescence, X-ray diffraction and multispectral imaging on Mars. *Science Advances* **8**, 47. <https://doi.org/10.1126/sciadv.abp9084>.
- Tosca JA and Knoll AH (2009) Juvenile chemical sediments and the long term persistence of water at the surface of Mars. *Earth and Planetary Science Letters* **286**, 379–386. <https://doi.org/10.1016/j.epsl.2009.07.004>.
- Treiman AH, Amundsen HEF, Blake DF and Bunch T (2002) Hydrothermal origin for carbonate globules in Martian meteorite ALH84001: a terrestrial analogue from Spitsbergen (Norway). *Earth and Planetary Science Letters* **204**, 323–332. [http://doi.org/10.1016/S0012-821X\(02\)00998-6](http://doi.org/10.1016/S0012-821X(02)00998-6).
- Treiman AH, Robinson KL, Blake DF and Bish D (2010) ‘Mineralogy determinations by CheMin XRD, tested on ultramafic rocks.’ LPSC 41, The Woodlands, TX, March 1–5, 2010. Abstr. #1472, Available at <https://www.lpi.usra.edu/meetings/lpsc2010/pdf/1472.pdf>
- Treiman AH, Morris RV, Agresti DG, Graff TG, Achilles CN, Rampe EB, Bristow TF, Blake DF, Vaniman DT, Bish DL, Chipera SJ, Morrison SM and Downs RT (2014) Ferrian saponite from the Santa Monica Mountains (California, USA, Earth): characterization as an analog for clay minerals on Mars with application to Yellowknife Bay in Gale crater. *American Mineralogist* **99**, 2234–2250. <https://doi.org/10.2138/am-2014-4763>.
- Tyler SA and Barghoorn ES (1954) Occurrence of structurally preserved plants in Pre-Cambrian rocks of the Canadian Shield. *Science* **119**, 606–608.
- VanBommel SJ, Gellert R, Berger JA, Campbell JL, Thompson LM, Edgett KS, McBride MJ, Minitti ME, Prader I and Boyd NI (2016) Deconvolution of distinct lithology chemistry through oversampling with the Mars Science Laboratory Alpha Particle X-Ray Spectrometer. *X-Ray Spectrometry* **45**, 155–161. <https://doi.org/10.1002/xrs.2681>.
- Vaniman DT, Bish DL, Ming DW, Bristow TF, Morris RV, Blake DF, Chipera SJ, Morrison SM, Treiman AH, Rampe EB, Rice M, Achilles CN, Grotzinger JP, McLennan SM, Williams J, Bell III JF, Newsom HE, Downs RT, Maurice S, Sarrazin P, Yen AS, Morookian JM, Farmer JD, Stack K, Milliken RE, Ehlmann BL, Sumner D and the Mars Science Laboratory Science Team (2013) Mineralogy of a mudstone at Yellowknife Bay, Gale crater, Mars. *Science* **343**, 1243480. <https://doi.org/10.1126/science.1243480>
- Walroth RC, Sarrazin P, Blake DF, Thompson K, Gailhanou M, Bristow T, Marchis F, Downs R, Webb S and Chalumeau C (2019) ‘MapX: full-field X-ray fluorescence imager for *in-situ* habitability and biosignature investigations.’ *Ninth Intl. Conf. on Mars*, Pasadena, CA, July 22–26, 2019. LPI Contribution No. 2089, id.6329. Available at <https://ui.adsabs.harvard.edu/abs/2019LPICo2089.6329W>
- Walter P, Sarrazin P, Gailhanou M, Herrouard D, Verney A and Blake DF (2018) Full-field XRF instrument for cultural heritage: application to the study of a Caillebotte painting. *X-Ray Spectrometry* **48**, 274–281. <https://doi.org/10.1002/xrs.2841>.